smeared band was detected; this shows that intact 80S ribosomes were purified, with no degradation incurred during purification. Simultaneously, the ribosomal proteins of the 80S ribosomes from the normal strain and the NAT mutants were separated by SDS-PAGE and detected by CBB staining (Fig. 1B). It should be noted that CBB-stained ribosomal protein gel images from the normal strain and the NAT mutants were identical. Then, gel-separated protein bands were in gel-digested by trypsin and the resulting peptides were analyzed by MS/MS to identify the proteins (Supplementary Table 1). A total of 50 ribosomal proteins were identified, but no non-ribosomal proteins were found, indicating that the ribosomes were highly purified.

Next, the ribosomal proteins were separated using 2-DE and detected by CBB staining (Fig. 1C). A total of 59 protein spots were detected on the 2-DE gel. These proteins were in gel-digested with trypsin, and the resultant peptides were analyzed by MS/MS to identify 60 ribosomal proteins (Fig. 1C and Supplementary Table 2). Interestingly, ribosomal proteins S5 (spots 5 and 6) and S10 (spots 54, 55, and 56) were identified in more than two spots having different isoelectric points, suggesting that these ribosomal proteins may be modified with a modification group such as phosphate.

3.2. *Identification of N^{α}-acetylated ribosomal proteins*

To identify which of the NATs acetylates which ribosomal proteins, we analyzed the ribosomal proteins in the normal strain and the NAT mutants using 2D-DIGE, and found that

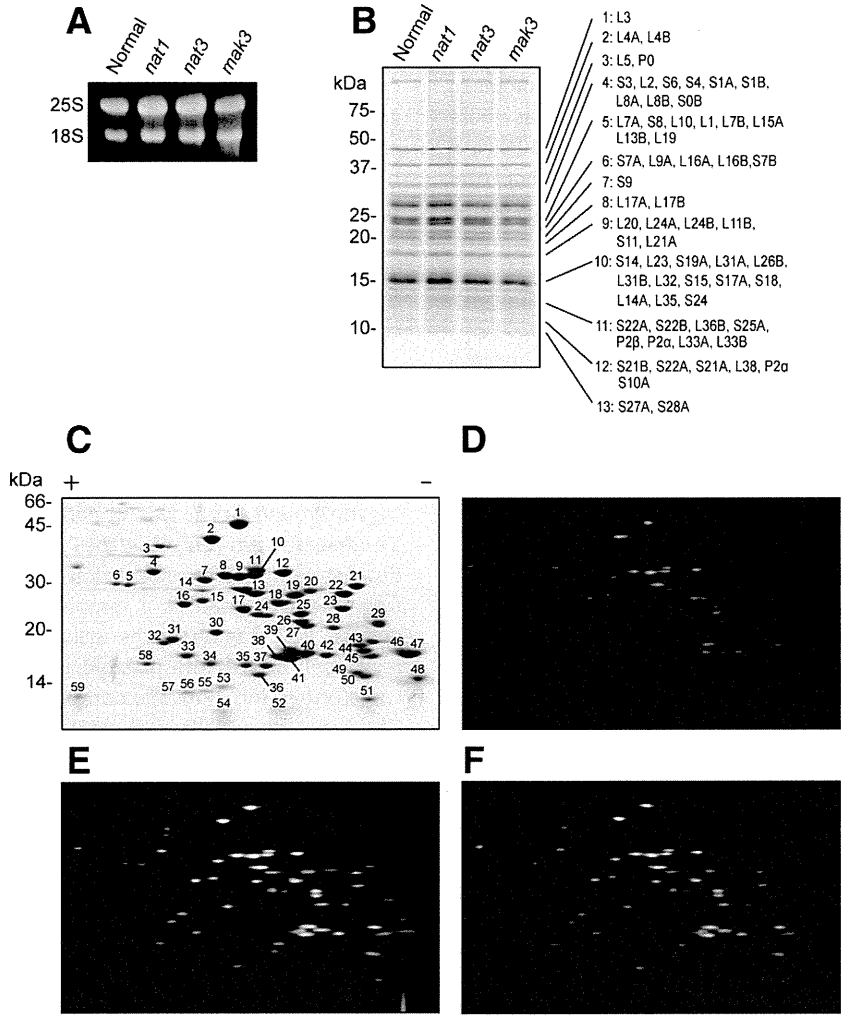

Fig. 1 – Analysis of rRNAs and N^{α}-acetylated ribosomal proteins by 2D-DIGE. (A) Purified rRNA from yeast 80S ribosomes was separated by agarose gel electrophoresis and stained with ethidium bromide. (B) Purified ribosomal proteins from yeast 80S ribosomes were separated by SDS-PAGE and stained with CBB R-250. The details of MS data using an ESI-LIT-TOF MS was shown in Supplementary Table 1. (C) Purified ribosomal proteins from yeast 80S ribosomes were separated by 2-DE using acid-urea electrophoresis in the first dimension and SDS-PAGE in the second dimension and stained with CBB R-250. Protein spots identified by an ESI-Q-TOF-MS are numbered and their details were indicated in Supplementary Table 2. (D–F) Identification of the N^{α}-acetylated ribosomal proteins from the *nat1*, *nat3*, and *mak3* mutants, respectively. Equal amounts of purified ribosomal proteins from the normal strain and the NAT mutant were labeled with Cy3 and Cy5 respectively. The Cy-labeled ribosomal proteins from the two strains were separated on the same 2-DE gel and the Cy3- and Cy5-images were compared. The N^{α}-acetylated ribosomal proteins are shown in Table 1.

Table 1 – N^{α}-Acetylation of ribosomal proteins.

Subunit	Protein	MW (kDa) [a]	pI [a]	2-DE [b]	TOF-MS [c]	DIGE	NAT
60S	P0	33.7	4.6	–	–	–	–
	P1 A/B	10.9/10.6	3.6/3.7	–	●/–	–	–
	P2 A/B	10.7/11.1	3.8/3.9	–	O/O	–	–
	L1 A/B [d]	24.5/24.5	9.7/9.7	–	●/●	●/●	NatA
	L2 A/B [d]	27.4/27.4	11.1/11.1	O/–	–	O/O	–
	L3	43.7	10.3	O	–	O	–
	L4 A/B	39.0/39.0	10.6/10.6	●/–	–	●/●	NatA
	L5	33.7	6.4	–	–	O	–
	L6 A/B	19.9/20.0	10.1/10.1	–	●/–	O/O	–
	L7 A/B	27.6/27.7	10.2/10.2	O/–	O/–	O/O	–
	L8 A/B	28.1/28.1	10.0/10.0	O/–	O/–	O/O	–
	L9 A/B	21.6/21.7	9.7/10.5	–	–	O/–	–
	L10	25.4	10.8	–	O	–	–
	L11 A/B	19.7/19.7	9.9/9.9	●	●/●	●/●	NatA
	L12 A/B [d]	17.8/17.8	9.4/9.4	–	–	O/O	–
	L13 A/B	22.5/22.5	11.2/11.7	–	–	O/–	–
	L14 A/B	15.2/15.2	10.4/11.6	–	●/–	●/–	NatA
	L15 A/B [d]	24.4/24.4	11.4/12.0	O/–	–	O/–	–
	L16 A/B	22.2/22.2	10.5/10.5	●/●	–/●	●/●	NatA
	L17 A/B	20.5/20.5	10.9/10.9	–	O/–	O/O	–
	L18 A/B [d]	20.6/20.6	11.7/11.7	–	–	O/O	–
	L19 A/B [d]	21.7/21.7	11.4/11.4	O/–	–	O/O	–
	L20 A/B	20.4/20.4	10.3/10.3	–	–	O/O	–
	L21 A/B	18.2/18.3	10.4/11.2	–	O/–	O/–	–
	L22 A/B	13.7/13.8	5.9/6.0	–	O/–	O/–	–
	L23 A/B [d]	14.5/14.5	10.3/10.3	–	–	●/●	NatA
	L24 A/B	17.6/17.5	11.3/11.4	–	–	O/O	–
	L25	15.7	10.1	O	O	O	–
	L26 A/B	14.2/14.2	11.4/10.5	–	–/O	–/O	–
	L27 A/B	15.5/15.5	10.4/11.2	–	O/–	O/–	–
	L28	16.7	10.5	–	O	O	–
	L29	6.7	12	–	O	–	–
	L30	11.4	9.8	–	O	O	–
	L31 A/B	12.9/13.0	10.0/10.0	–	O/–	O/O	–
	L32	14.8	11.2	–	O	O	–
	L33 A/B	12.1/12.2	11.1/11.1	–	●/–	O/O	–
	L34 A/B	13.6/13.6	11.6/11.6	–	–	–	–
	L35 A/B [d]	13.9/13.9	10.6/10.6	–	–	O/O	–
	L36 A/B	11.1/11.1	12.2/11.6	–	●/ O	–/O	–
	L37 A/B	9.8/9.7	12.2/12.3	–	–	–	–
	L38	8.8	10.9	–	O	O	–
	L39	6.3	–	–	O	–	–
	L40 A/B [d]	14.5/14.5	10.6/10.6	–	–	–	–
	L41 A/B [d]	3.3/3.3	–	–	–	–	–
	L42 A/B [d]	12.2/12.2	11.4/11.4	–	–/O	–	–
	L43 A/B [d]	10.0/10.0	11.2/11.4	–	–	–	–
40S	S0 A/B	28.0/28.0	4.5/4.5	–	●/–	–	–
	S1 A/B	28.7/28.8	10.0/10.0	●/–	●/–	O/O	NatA
	S2	27.4	10.4	●	●	●	NatA
	S3	26.5	9.4	O	O	O	–
	S4 A/B [d]	29.3/29.3	10.1/10.1	–	O/–	O/O	–
	S5	25	8.6	●	●	●	NatA
	S6 A/B [d]	27.0/27.0	10.4/10.4	–	–	O/O	–
	S7 A/B	21.6/21.6	9.8/9.9	●/–	●/●	●/●	NatA
	S8 A/B [d]	22.5/22.5	10.7/10.7	–	O/–	O/O	–
	S9 A/B	22.4/22.3	10.8/10.1	–	–	–/O	–
	S10 A/B	12.7/12.7	8.7/9.92	–	O/O	O/–	–
	S11 A/B [d]	17.7/17.7	10.8/10.8	–	●/–	●/●	NatA
	S12	15.8	4.5	–	–	–	–
	S13	17	10.4	–	O	O	–
	S14 A/B	14.5/14.6	10.7/11.3	●/–	●/–	●/–	NatA
	S15	16	10.7	–	●	●	NatA
	S16 A/B [d]	15.8/15.8	10.3/10.3	●/–	●/–	●/●	NatA

(continued on next page)

Table 1 (*continued*)

Subunit	Protein	MW (kDa)[a]	pI[a]	2-DE[b]	TOF-MS[c]	DIGE	NAT
40S	S17 A/B	15.8/15.8	10.5/11.3	–	–	●/–	NatA
	S18 A/B[d]	17.0/17.0	10.3/10.3	–	●/●	●/●	NatA
	S19 A/B	15.9/15.9	9.6/10.5	–	–/O	O/–	–
	S20	13.9	9.5	–	●	●	NatA
	S21 A/B	9.7/9.5	5.8/5.8	–	●/●	●/●	NatB
	S22 A/B	14.6/14.6	9.9/9.9	–	O/–	O/O	–
	S23 A/B[d]	16.0/16.0	11.5/11.5	–	–	–	–
	S24 A/B[d]	15.3/15.3	10.5/10.5	●/–	●/–	●/●	NatA
	S25 A/B	12.0/12.0	10.3/11.1	–	–	O/–	–
	S26 A/B	13.5/13.4	10.8/11.6	–	–	O/–	–
	S27 A/B	8.9/8.9	9.4/9.5	–	O/O	O/–	–
	S28 A/B	7.6/7.6	10.8/11.4	–	●/●	●/–	NatB
	S29 A/B	6.7/6.7	11.1/10.8	–	O/O	–	–
	S30 A/B	7.1/7.1	12.2/12.2	–	O/O	–	–
	S31	17.2	10.7	–	–	–	–
Total	78			18	50	60	

●: N^{α}-Acetylated ribosomal protein. O: identified ribosomal protein.
[a] The calculated molecular weight and pI of ribosomal proteins were obtained from SWISS-PROT database.
[b] N^{α}-Acetylated ribosomal proteins were identified by 2-DE with an amino acid sequencer (Takakura et al.).
[c] N^{α}-Acetylated ribosomal proteins were identified by MALDI-TOF-MS (Arnold et al.).
[d] These ribosomal proteins A/B are used for duplicated genes that code proteins with identical sequence.

the following 17 ribosomal proteins in the *nat1* mutant were different in electrophoretic mobility from those in the normal strain (Fig. 1D); S2, S5, S7AB, S11, S14A, S15, S16, S17A, S18, S20, and S24 from the 40S subunit and L1, L4AB, L11B, L14A, L16AB, and L23 from the 60S subunit. These ribosomal proteins prepared from the *nat1* mutant had a shift toward the alkaline side of the gel that corresponds to the change in the protein isoelectric point expected from the lack of N^{α}-acetylation of an α-amino group. In addition, in a sample from the *nat3* mutant two ribosomal proteins, S21 and S28, had altered isoelectric points (Fig. 1E). However, no ribosomal proteins from the *mak3* mutant had changed isoelectric points (Fig. 1F). Although N^{α}-acetylation of ribosomal proteins was reported previously [12–14], this is the first time that ribosomal proteins L23 and S17 have been shown to be the substrates of NatA. The identified N^{α}-acetylated ribosomal proteins are listed in Table 1.

3.3. *Effects of the NAT deletion on cell growth*

It is well known that deletions or mutations of ribosomal protein genes influences both cell growth and temperature-sensitivity. We investigated the growth of the NAT mutants in the YPD medium at 30 °C (Fig. 2A). The doubling time was 1.4, 1.7, 4.0 and 1.4 h for the normal strain, *nat1*, *nat3*, and *mak3* mutants, respectively. The growth of the *nat1* and *nat3* mutants was decreased as compared to the normal strain, while the growth of the mak3 mutant remained unaltered, suggesting that the lack of protein N^{α}-acetylation by NatA and NatB affects cell growth. Next, we investigated the temperature sensitivity of the NAT mutants using 10-fold dilution spot assays performed on YPD plates at three different temperatures (20, 30, and 37 °C) (Fig. 2B). Growth of the normal and the NAT mutants was not significantly affected at 30 °C. In contrast, the *nat1* and *nat3* mutants showed slow growth phenotype at 37 °C.

3.4. *Effect of ribosomal protein N^{α}-acetylation on polyU-dependent poly-(Phe) synthesis*

The slower growth of the *nat1* and *nat3* mutants suggests that ribosomal protein N^{α}-acetylation may have an effect on protein synthesis, the most important function of ribosomes. Changes in the structure or function of yeast ribosomes are known to affect cell growth rate at a range of temperatures. In order to study the effect of ribosomal protein N^{α}-acetylation on protein synthesis, we performed polyU-dependent poly-(Phe) synthesis assays (Fig. 2C). The results demonstrated that the protein synthesis activities of 80S ribosomes purified from the *nat1* and *nat3* mutants were decreased by about 27% and 23%, respectively, as compared to the normal ribosomes. Thus, decreased protein synthesis activities in the *nat1* and the *nat3* mutants could be explained by the lack of N^{α}-acetylation of at least two or more ribosomal proteins from the list of 19 identified acetylated ribosomal protein (see above).

3.5. *Effect of the N^{α}-acetylation on polysome formation*

Polysome analysis in sucrose gradient is used to detect possible defects in ribosomal subunit assembly and proper organization of the ribosome chains that may cause protein synthesis alteration. As we observed decreased translation in the *nat1* and the *nat3* mutants it is possible that ribosome assembly or polysome organization is affected in the mutants. Therefore, we fractionated cell extracts from the normal and the NAT mutants in 7–47% sucrose density-gradient (Fig. 2D). Although the *nat1* and *mak3* mutants exhibited polysome profiles similar to the one from the normal strain, the *nat3* mutant clearly showed a defect in 80S ribosome assembly as the corresponding 80S ribosome peak was significantly decreased and 60S subunit peak was abnormally high. While no disruption of the polysome chains was observed, it appears that the altered ratio of 60S subunits to 80S ribosomes is either

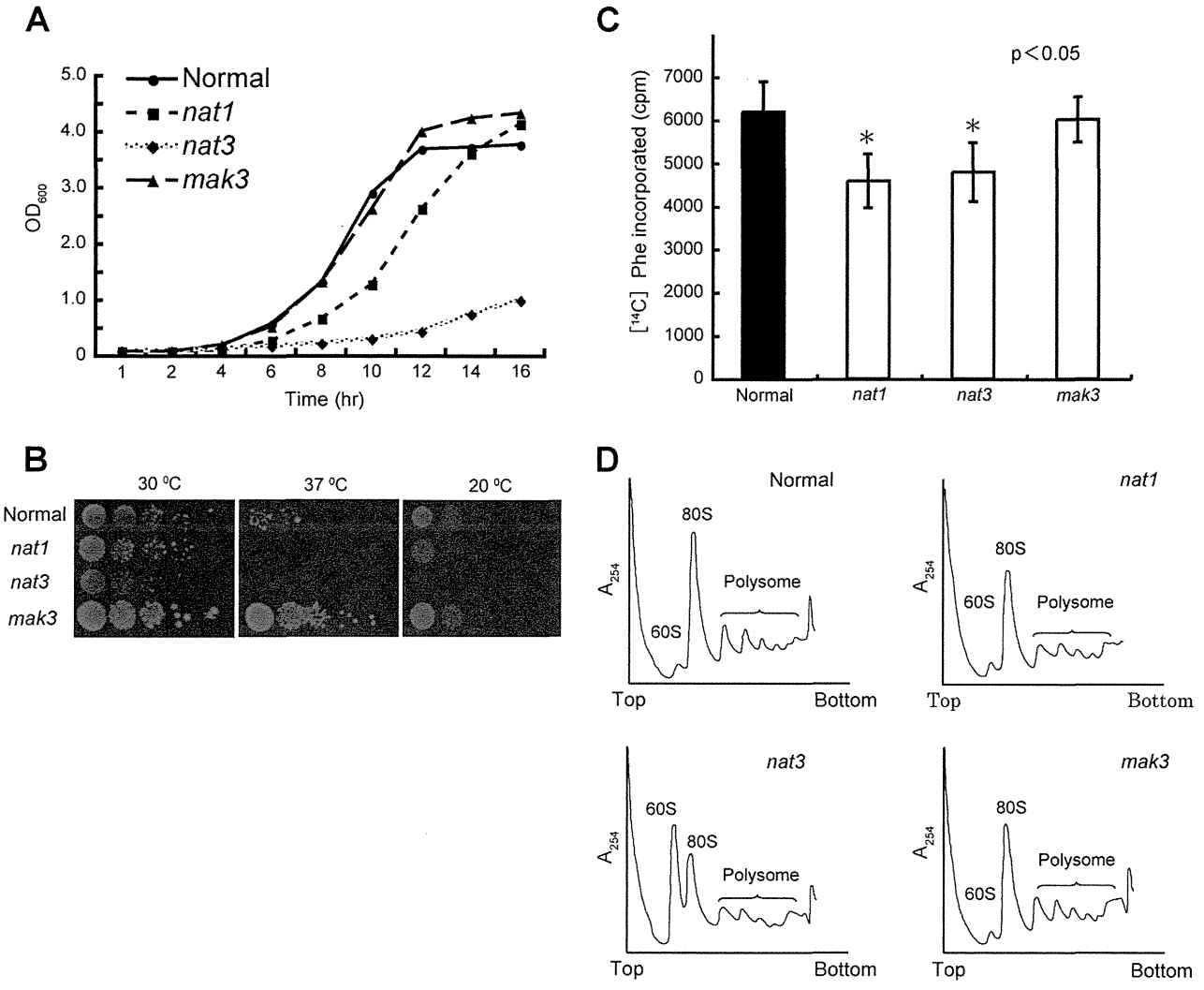

Fig. 2 – The effect of N^{α}-acetylation on cell growth and protein synthesis. (A) Growth curves of the normal strain and the NAT mutants. All strains were cultured in YPD at 30 °C until stationary phase. The absorbance of each culture was measured at 600 nm every 2 h. (B) Effect of three different temperatures (20, 30 and 37 °C) on the growth of the normal strain and the NAT mutants. Freshly grown yeast colonies were suspended in water, and 1/10 dilutions containing the same number of cells were spotted onto YPD plates. Spotted plates were incubated at 20, 30 and 37 °C for 3 to 4 days. (C) Effect of N^{α}-acetylation on polyU-dependent poly (Phe) synthesis. Purified 80S ribosomes from the normal strain and the NAT mutants were added to assay mixtures containing soluble factor S-100 from the normal strain and radioactive Phe residues, and incubated at 30 °C for 30 min. The radioactivity of the insoluble fraction, a measure of the incorporation of radioactive amino acids, was determined by liquid scintillation counter. The value shown in the figure was calculated by subtracting the value of the activity at 0 min. (D) The polysome profiles of the normal strain and the NAT mutants. Cytoplasmic extracts from the normal and the mutant strains were loaded onto 7–47% sucrose gradients, centrifuged, and fractionated. The fractions were collected from the top to the bottom with continuous A_{254} monitoring.

due to a failure to form 80S ribosomes or due to disruption in 40S subunit assembly. Thus, it is possible that decreased protein synthesis activity in the *nat3* mutant is at least in part due to a defect in ribosome assembly, whereas the altered activity in the *nat1* mutant is due to a difference of the fully assembled 80S ribosome.

3.6. *Sensitivity of the nat1 mutant to translation inhibitors*

In order to obtain more data on how NatA ribosomal protein N^{α}-acetylation affects ribosomal functions, we performed 1/10-dilution spot assays using YPD plates containing various antibiotics that bind to the ribosome and inhibit translation (Fig. 3A). We found that neither the normal strain nor the *nat1* mutant was sensitive to puromycin, which is known to cause premature chain termination during translation. However, both of the normal strain and the *nat1* mutant were sensitive to anisomycin and cycloheximide. Anisomycin is a competitive inhibitor of A-site binding that sterically hinders positioning of the acceptor end of A-site tRNA in the peptidyl transferase center (PTC) on the 60S subunit of the ribosome and cycloheximide is known to interfere with the translocation step in protein synthesis by blocking translational elongation. These

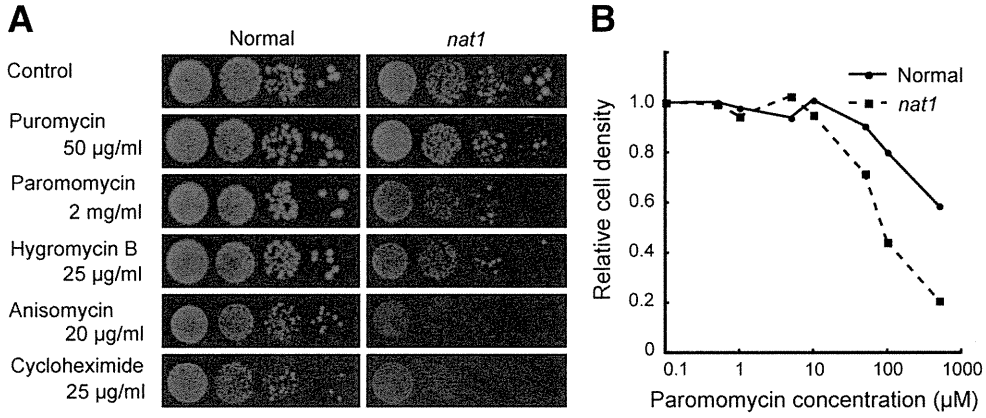

Fig. 3 – The effect of the NatA deletion on sensitivity to translation inhibitors. (A) The effect of various antibiotics on the growth of the normal strain and the *nat1* mutant. Freshly grown yeast colonies were suspended in water, and 1/10 dilutions starting at 0.1 OD_{600} were spotted onto YPD plates containing the indicated antibiotics. Spotted plates were incubated at 30 °C for 4 days. (B) The effect of paromomycin on growth of the normal strain and the *nat1* mutant. Freshly grown yeast colonies were cultured in YPD containing increasing concentrations of antibiotics until the culture without antibiotic reached an OD_{600} of 1–1.5, which was taken as 1.0.

results suggest that N^{α}-acetylation of ribosomal proteins by NatA has no specific effect on translocation or peptidyl transferase activity.

On the other hand, both paromomycin and hygromycin caused a specific decrease in the growth of the *nat1* mutant as compared to the normal strain. Therefore, we examined the effect of various paromomycin concentrations on growth of the *nat1* mutant (Fig. 3B) and found that sensitivity to paromomycin is increasing at higher antibiotic concentrations. Paromomycin is a translational error-inducing antibiotic that binds to the decoding center on the ribosome's 40S subunit and promotes conformational changes affecting formation of the codon–anticodon helix between mRNA and tRNA at the A-site. Thus, it appears that the N^{α}-acetylation of ribosomal proteins by NatA may be required to maintain a proper translational fidelity.

3.7. *The role of ribosomal protein N^{α}-acetylation in translational fidelity*

We investigated the *nat1* mutant's translational fidelity using a bicistronic reporter gene consisting of genes encoding a protein A peptide (14 kDa) and a FLAG peptide (1 kDa) (Fig. 4A). In this assay, if translation is accurate, the 14 kDa peptide is produced. If stop codon readthrough occurs, the 15 kDa peptide (which includes the FLAG tag) is produced. In the normal strain, we analyzed the affect of paromomycin on the level of a readthrough product in a concentration-dependent manner (Fig. 4B). We found that the readthrough product increased with increasing concentrations of paromomycin. Using this construct, we compared translational fidelity between the normal strain and the *nat1* mutant (Fig. 4C). The amount of a stop codon readthrough product in the *nat1* mutant was slightly higher than in the normal strain. Additionally, the level of the readthrough product in the *nat1* mutant was strongly influenced by the addition of paromomycin. Thus, N^{α}-acetylation by NatA is required for optimal translational termination. In addition, our reporter construct is useful for the analysis of translational fidelity in yeast.

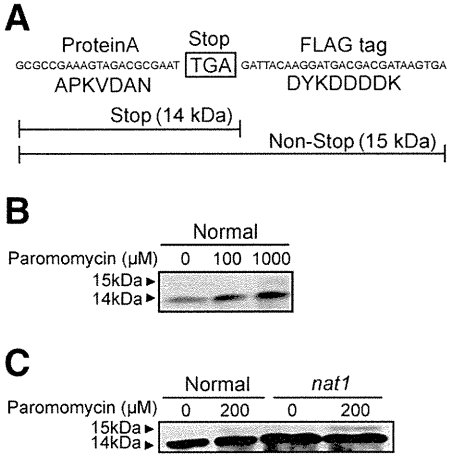

Fig. 4 – The role of ribosomal protein N^{α}-acetylation in translational readthrough activity. (A) The structure of the stop codon readthrough construct used in this study. The 14 kDa protein A fragment is a predominant translation product in the normal strain. The 14 kDa protein A fragment combined with the FLAG tag protein (1 kDa) which resulted in 15 kDa peptide is the mistranslated protein product. (B) Protein production in the normal strain with high concentration of paromomycin induced stop codon readthrough. Cells were grown in YPD containing the indicated concentration of paromomycin. Protein samples were loaded onto 15% SDS-PAGE and detected using Western blot with anti-peroxidase antibody. (C) Comparison of stop codon readthrough activity between the normal strain and the *nat1* mutant.

4. Discussion

Genome sequencing has revealed that yeast contains 137 ribosomal protein genes, encoding 78 unique ribosomal proteins with 59 encoded by duplicate genes [27]. Takakura et al. detected a total of 44 ribosomal proteins in the yeast 80S ribosome by 2-DE using acid-urea gel electrophoresis in the first dimension and SDS-PAGE in the second dimension, and identified 14 ribosomal proteins which were N^{α}-acetylated by NatA using Edman degradation [12]. Arnold et al. found that 30 of the identified 68 ribosomal proteins, including the isoforms, were N-terminally acetylated by NatA, NatB, or NatC using shotgun analysis by MALDI-TOF MS [13]. In the present study, we applied 2D-DIGE and MS/MS to identify the N^{α}-acetylated ribosomal proteins of the yeast 80S ribosome. By these techniques, we detected N^{α}-acetylated proteins and their non-acetylated counterparts as pairs of differently colored spots with slightly different isoelectric points. The numbers of ribosomal proteins and N^{α}-acetylated ribosomal proteins, not including isoforms, were 60 and 19, respectively, showing that we detected 77% of the 78 ribosomal proteins encoded and 83% of the known 69 basic ribosomal proteins (pI > 7). We did not detect the remaining 18 ribosomal proteins by 2D-DIGE, because of low molecular weight (MW < 8000 Da) or isoelectric point (pI < 5).

Nevertheless, this is the first report to describe the use of 2D-DIGE and MS/MS techniques in the differential display analysis of N^{α}-acetylated and non-N^{α}-acetylated ribosomal proteins and we detected more ribosomal proteins and N^{α}-acetylated ribosomal proteins than in the previous studies.

We also investigated the effect of the lack ribosomal protein N^{α}-acetylation on the ribosome function using the NAT mutants. The deletion of *MAK3* (component of NatC) did not affect ribosomal protein N^{α}-acetylation or protein synthesis. In the *nat3* (NatB) mutant, two ribosomal proteins lost the N^{α}-acetyl group, and the protein synthesis activity of purified ribosomes was decreased (Fig. 2). Although the abnormal accumulation of the 60S subunit and lower proportion of the 80S ribosome in the *nat3* mutant might contribute to the low protein synthesis activity of the ribosomes, its mechanism remains unknown. The deletion of *NAT1* (component of NatA) caused the loss of N^{α}-acetylation in 17 ribosomal proteins. The polysome formations of the normal strain and the *nat1* mutant were similar, but the protein synthesis activity of ribosomes purified from the *nat1* mutant was decreased (Fig. 2). In addition, the growth of the *nat1* mutant was decreased on YPD plates, containing the error-inducing antibiotics paromomycin and hygromycin (Fig. 3), and the *nat1* mutant translational readthrough activity was increased *in vivo* (Fig. 4). These results are in agreement with the data of Pezza et al. [28].

We assigned the N^{α}-acetylated proteins to the yeast 80S ribosome structure reported by Spahn et al. [29]. Most of the N^{α}-acetylated ribosomal proteins were located around the shoulder, the E-site, or the head on the 40S subunit (Fig. 5). The NatA N^{α}-acetylated ribosomal proteins around the shoulder of the ribosome are conserved between *Escherichia coli* (*E. coli*) and yeast. Among them, *E. coli* ribosomal proteins S4 (yeast ribosomal protein S9 homolog) and S5 (yeast ribosomal protein S2 homolog) contribute to streptomycin resistance [30,31]. Particularly, *E. coli* ribosomal protein S5 is involved in

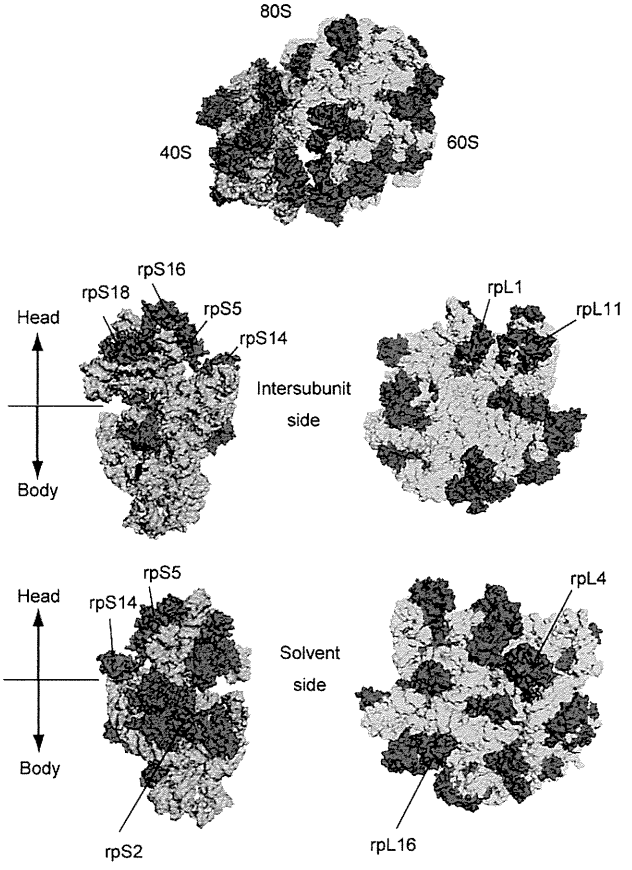

Fig. 5 – Location of NatA N^{α}-acetylated ribosomal proteins on the 80S ribosome structure. The 25S rRNA is in light blue, the 18S rRNA is in green, the non-N^{α}-acetylated ribosomal proteins are in dark blue, and the N^{α}-acetylated ribosomal proteins are in red. The graphic visualization was done with the program PyMol (PDB ID: 1S1H and 1S1I).

tRNA selection and translational fidelity [32]. To determine whether the lack of yeast ribosomal protein S2 N^{α}-acetylation affects translational readthrough, we tested the ribosomal protein S2 mutant with altered N-terminal residue and lacking acetylation. In this experiment, a penultimate serine residue was replaced with tyrosine by mutating the corresponding locus of genomic DNA encoding for S2, resulting in expression of non-N^{α}-acetylated S2 in the mutant. The results show that non-N^{α}-acetylated S2 was not sensitive to paromomycin, suggesting that the N^{α}-acetylation of other ribosomal proteins besides S2 is necessary for translational fidelity in yeast.

The function of the E-site, at which NatA N^{α}-acetylated ribosomal proteins S5 and S14 are located, is to release tRNA and mRNA from the ribosome [33]. The E-site is allosterically coupled to the A-site, and this coupling controls the ability of the ribosome to discriminate between cognate and noncognate tRNAs at the A-site [34]. According to previous reports, the N-terminal domain (~46 amino acids) of yeast ribosomal protein S5 plays an important role in initiation of translation and translational fidelity [35,36]. It is possible that loss of the N^{α}-acetylation of the ribosomal proteins located at the E site contributes to the decreased translational fidelity.

In addition, the N^{α}-acetylated ribosomal proteins S15, S16, S18, and S20 are located at the head of the 40S subunit. There are no reports describing the role of these ribosomal proteins in protein synthesis. However, the present data suggest that the ribosomal proteins located at the ribosome head may be involved in the protein synthesis function as the lack of N^{α}-acetylation of these protein affect protein synthesis.

In yeast, ribosomal proteins L12 and S25 are methylated by N-terminal methyltransferase Tae1p [37]. Interestingly, *TAE1* deletion has similar phenotypes to some of the NatA deletion phenotypes, for example, protein synthesis activity is decreased and paromomycin sensitivity is increased [38]. N-terminal modification causes neutralization of the positive charge on the N-terminal amino group of the protein. Therefore, the lack of N-terminal acetylation and the presence of a positive charge on the N-terminus may affect the interaction between the various components of the ribosome, such as ribosomal proteins, rRNA, and tRNA, causing defects in translation function.

In general, the lack of N^{α}-acetylation can cause any of the following degrees of effects: (i) no substantial change of function or stability; (ii) partial diminution of function or stability; (iii) complete or almost complete loss of function or stability. For example, yeast iso-1-cytochrome c, which is normally not N^{α}-acetylated, is not affected by N^{α}-acetylation introduced by mutation of the N-terminal region [5]. An opposite example, the lack of N^{α}-acetylation of the killer viral coat protein Gag causes a 5 to 10-fold reduction of the protein [10]. However, the function or stability of most proteins is less affected by the lack of N^{α}-acetylation, as examined in detail with actin and tropomyosin [11]. The lack of N^{α}-acetylation of actin results in only approximately 50% of the ATPase activation. We wish to emphasize that *act1-Δ* mutants are lethal, as are deletions of genes that encode any essential protein. In this regard, genes encoding ribosomal proteins are essential, as are hundreds of other genes, suggesting that the lack of N^{α}-acetylation of proteins in mutants of NatA, NatB, and NatC cause only partial defects. Also, the concomitant defects in NatA and NatB mutants make it difficult to assign the functions to specific ribosomal proteins.

Supplementary materials related to this article can be found online at doi:10.1016/j.jprot.2010.12.007.

Acknowledgements

This work was supported in part by Special Coordination Funds for Promoting Science and Technology "Creation of Innovation Centers for Advanced Interdisciplinary Research Areas" (to H.H.) and in part by the National Institutes of Health Grant R01 GM12702 (to F.S.).

REFERENCES

[1] Frottin F, Martinez A, Peynot P, Mitra S, Holz RC, Giglione C, et al. The proteomics of N-terminal methionine cleavage. Mol Cell Proteomics 2006;5:2336–49.

[2] Bradshaw RA, Brickey WW, Walker KW. N-terminal processing: the methionine aminopeptidase and N alpha-acetyl transferase families. Trends Biochem Sci 1998;23:263–7.

[3] Gautschi M, Just S, Mun A, Ross S, Rücknagel P, Dubaquié Y, et al. The yeast N(alpha)-acetyltransferase NatA is quantitatively anchored to the ribosome and interacts with nascent polypeptides. Mol Cell Biol 2003;23:7403–14.

[4] Arnesen T, Van Damme P, Polevoda B, Helsens K, Evjenth R, Colaert N, et al. Proteomics analyses reveal the evolutionary conservation and divergence of N-terminal acetyltransferases from yeast and humans. Proc Natl Acad Sci USA 2009;106:8157–62.

[5] Polevoda B, Sherman F. N-terminal acetyltransferases and sequence requirements for N-terminal acetylation of eukaryotic proteins. J Mol Biol 2003;325:595–622.

[6] Polevoda B, Sherman F. Composition and function of the eukaryotic N-terminal acetyltransferase subunits. Biochem Biophys Res Commun 2003;308:1–11.

[7] Polevoda B, Hoskins J, Sherman F. Properties of Nat4, an N (alpha)-acetyltransferase of *Saccharomyces cerevisiae* that modifies N termini of histones H2A and H4. Mol Cell Biol 2009;29:2913–24.

[8] Geissenhöner A, Weise C, Ehrenhofer-Murray AE. Dependence of ORC silencing function on NatA-mediated Nalpha acetylation in *Saccharomyces cerevisiae*. Mol Cell Biol 2004;24: 10300–12.

[9] Wang X, Connelly JJ, Wang CL, Sternglanz R. Importance of the Sir3 N terminus and its acetylation for yeast transcriptional silencing. Genetics 2004;168:547–51.

[10] Tercero JC, Wickner RB. MAK3 encodes an N-acetyltransferase whose modification of the L-A gag NH2 terminus is necessary for virus particle assembly. J Biol Chem 1992;267: 20277–81.

[11] Polevoda B, Cardillo TS, Doyle TC, Bedi GS, Sherman F. Nat3p and Mdm20p are required for function of yeast NatB N^{α}-terminal acetyltransferase and of actin and tropomyosin. J Biol Chem 2003;278:30686–97.

[12] Takakura H, Tsunasawa S, Miyagi M, Warner JR. NH_2-terminal acetylation of ribosomal proteins of *Saccharomyces cerevisiae*. J Biol Chem 1992;267:5442–5.

[13] Arnold RJ, Polevoda B, Reilly JP, Sherman F. The action of N-terminal acetyltransferases on yeast ribosomal proteins. J Biol Chem 1999;274:37035–40.

[14] Lee SW, Berger SJ, Martinović S, Pasa-Tolić L, Anderson GA, Shen Y, et al. Direct mass spectrometric analysis of intact proteins of the yeast large ribosomal subunit using capillary LC/FTICR. Proc Natl Acad Sci USA 2002;99:5942–7.

[15] Nilsson J, Sengupta J, Gursky R, Nissen P, Frank J. Comparison of fungal 80S ribosomes by cryo-EM reveals diversity in structure and conformation of rRNA expansion segments. J Mol Biol 2007;369:429–38.

[16] Dresios J, Panopoulos P, Synetos D. Eukaryotic ribosomal proteins lacking a eubacterial counterpart: important players in ribosomal function. Mol Microbiol 2006;59:1651–63.

[17] Planta RJ, Mager WH. The list of cytoplasmic ribosomal proteins of *Saccharomyces cerevisiae*. Yeast 1998;14:471–7.

[18] Blanchard SC, Cooperman BS, Wilson DN. Probing translation with small-molecule inhibitors. Chem Biol 2010;17: 633–45.

[19] Wilson DN, Nierhaus KH. Ribosomal proteins in the spotlight. Crit Rev Biochem Mol Biol 2005;40:243–67.

[20] Ruvinsky I, Sharon N, Lerer T, Cohen H, Stolovich-Rain M, Nir T, et al. Ribosomal protein S6 phosphorylation is a determinant of cell size and glucose homeostasis. Genes Dev 2005;19:2199–211.

[21] Tchórzewski M, Boguszewska A, Dukowski P, Grankowski N. Oligomerization properties of the acidic ribosomal P-proteins from *Saccharomyces cerevisiae*: effect of P1A protein phosphorylation on the formation of the P1A-P2B hetero-complex. Biochim Biophys Acta 2000;1499:63–73.

[22] Ren J, Wang Y, Liang Y, Zhang Y, Bao S, Xu Z. Methylation of ribosomal protein S10 by protein–arginine methyltransferase 5 regulates ribosome biogenesis. J Biol Chem 2010;285:12695–705.
[23] Shin HS, Jang CY, Kim HD, Kim TS, Kim S, Kim J. Arginine methylation of ribosomal protein S3 affects ribosome assembly. Biochem Biophys Res Commun 2009;385:273–8.
[24] Ohn T, Kedersha N, Hickman T, Tisdale S, Anderson P. A functional RNAi screen links O-GlcNAc modification of ribosomal proteins to stress granule and processing body assembly. Nat Cell Biol 2008;10:1224–31.
[25] Graham John M, David Rickwood. Subcellular fractionation: a practical approach. IRL Press at Oxford University Press; 1997.
[26] Liang XH, Liu Q, Fournier MJ. rRNA modifications in an intersubunit bridge of the ribosome strongly affect both ribosome biogenesis and activity. Mol Cell 2007;28:965–77.
[27] Link AJ, Eng J, Schieltz DM, Carmack E, Mize GJ, Morris DR, et al. Direct analysis of protein complexes using mass spectrometry. Nat Biotechnol 1999;17:676–82.
[28] Pezza JA, Langseth SX, Raupp Yamamoto R, Doris SM, Ulin SP, Salomon AR, et al. The NatA acetyltransferase couples Sup35 prion complexes to the [PSI+] phenotype. Mol Biol Cell 2009;20:1068–80.
[29] Spahn CM, Gomez-Lorenzo MG, Grassucci RA, Jørgensen R, Andersen GR, Beckmann R, et al. Domain movements of elongation factor eEF2 and the eukaryotic 80S ribosome facilitate tRNA translocation. EMBO J 2004;23:1008–19.
[30] Andersson DI, Bohman K, Isaksson LA, Kurland CG. Translation rates and misreading characteristics of rpsD mutants in *Escherichia coli*. Mol Gen Genet 1982;187:467–72.
[31] Piepersberg W, Böck A, Wittmann HG. Effect of different mutations in ribosomal protein S5 of *Escherichia coli* on translational fidelity. Mol Gen Genet 1975;140:91–100.
[32] Ogle JM, Murphy FV, Tarry MJ, Ramakrishnan V. Selection of tRNA by the ribosome requires a transition from an open to a closed form. Cell 2002;111:721–32.
[33] Carter AP, Clemons WM, Brodersen DE, Morgan-Warren RJ, Wimberly BT, Ramakrishnan V. Functional insights from the structure of the 30S ribosomal subunit and its interactions with antibiotics. Nature 2000;407:340–8.
[34] Nierhaus KH. Decoding errors and the involvement of the E-site. Biochimie 2006;88:1013–9.
[35] Galkin O, Bentley AA, Gupta S, Compton BA, Mazumder B, Kinzy TG, et al. Roles of the negatively charged N-terminal extension of *Saccharomyces cerevisiae* ribosomal protein S5 revealed by characterization of a yeast strain containing human ribosomal protein S5. RNA 2007;13:2116–28.
[36] Lumsden T, Bentley AA, Beutler W, Ghosh A, Galkin O, Komar AA. Yeast strains with N-terminally truncated ribosomal protein S5: implications for the evolution, structure and function of the Rps5/Rps7 proteins. Nucleic Acids Res 2010;38: 1261–72.
[37] Webb KJ, Lipson RS, Al-Hadid Q, Whitelegge JP, Clarke SG. Identification of protein N-terminal methyltransferases in yeast and humans. Biochemistry 2010;49:5225–35.
[38] Alamgir M, Eroukova V, Jessulat M, Xu J, Golshani A. Chemical-genetic profile analysis in yeast suggests that a previously uncharacterized open reading frame, YBR261C, affects protein synthesis. BMC Genomics 2008;9:583.

Cell Polarity in *Saccharomyces cerevisiae* Depends on Proper Localization of the Bud9 Landmark Protein by the EKC/KEOPS Complex

Yu Kato,[1] Hiroshi Kawasaki,[2] Yoshifumi Ohyama, Takashi Morishita,[3] Hiroshi Iwasaki,[4] Tetsuro Kokubo, and Hisashi Hirano

Department of Supramolecular Biology, Graduate School of Nanobioscience, Yokohama City University, Tsurumi-ku, Yokohama 230-0045, Japan

ABSTRACT In diploid *Saccharomyces cerevisiae* cells, bud-site selection is determined by two cortical landmarks, Bud8p and Bud9p, at the distal and proximal poles, respectively. Their localizations depend on the multigenerational proteins Rax1p/Rax2p. Many genes involved in bud-site selection were identified previously by genome-wide screening of deletion mutants, which identified *BUD32* that causes a random budding in diploid cells. Bud32p is an atypical kinase involved in a signaling cascade of Sch9p kinase, the yeast homolog of Akt/PKB, and a component of the EKC/KEOPS (endopeptidase-like, *k*inase, chromatin-associated/*k*inase, putative endopeptidase, and *o*ther *p*roteins of *s*mall size) complex that functions in telomere maintenance and transcriptional regulation. However, its role in bipolar budding has remained unclear. In this report, we show that the Sch9p kinase cascade does not affect bipolar budding but that the EKC/KEOPS complex regulates the localization of Bud9p. The kinase activity of Bud32p, which is essential for the functions of the EKC/KEOPS complex but is not necessary for the Sch9p signaling cascade, is required for bipolar bud-site selection. *BUD9* is necessary for random budding in each deletion mutant of EKC/KEOPS components, and *RAX2* is genetically upstream of EKC/KEOPS genes for the regulation of bipolar budding. The asymmetric localization of Bud9p was dependent on the complex, but Bud8p and Rax2p were not. We concluded that the EKC/KEOPS complex is specifically involved in the regulation of Bud9p localization downstream of Rax1p/Rax2p.

THE generation of cell polarity is important for the function of many cell types and underlies various processes such as cell division, differentiation, cell migration, cell–cell signaling, and fertilization (Freifelder 1960; Mooseker 1985; Hyman and White 1987; Bedinger *et al.* 1994; Chant and Pringle 1995; Kraut *et al.* 1996). In the budding yeast *Saccharomyces cerevisiae*, such polarization induces asymmetric growth to form a bud that becomes the daughter cell. Yeast cells polarize and divide by budding in two patterns: the axial pattern of haploid a/α-cells and the bipolar pattern of diploid a/α-cells. Axial budding in the haploid a/α-cells forms chain-like buds adjacent to the immediately preceding bud site, while bipolar budding in diploid a/α-cells forms cluster-like buds at either the proximal pole or its opposite distal pole. Alternate bud-site selections between proximal and distal poles usually occur in bipolar budding.

The establishment of yeast cell polarity undergoes three basic steps (Drubin and Nelson 1996). First, site selection occurs on the cell surface, a spatial landmark where cells will polarize. The bud sites during axial budding are marked with the axial landmarks Axl1p, Axl2p, Bud3p, and Bud4p (Fujita *et al.* 1994; Chant *et al.* 1995; Halme *et al.* 1996; Sanders and Herskowitz 1996). The bipolar landmarks Bud8p and Bud9p of the distal and proximal poles, respectively, determine the polarization axis of budding in diploid cells (Harkins *et al.* 2001). These cortical landmarks provide recognition sites for the Rsr1p/Bud2p/Bud5p GTPase

Copyright © 2011 by the Genetics Society of America
doi: 10.1534/genetics.111.128231
Manuscript received March 1, 2011; accepted for publication May 17, 2011
Supporting information is available online at http://www.genetics.org/content/suppl/2011/05/30/genetics.111.128231.DC1.
[1]Present address: Laboratory for Immunochaperons, Reasearch Center for Allergy and Immunology (RCAI), RIKEN Yokohama Institute, Suehiro-cho 1-7-22, Tsurumi-ku, Yokohama 230-0045, Japan
[2]Corresponding author: Department of Supramolecular Biology, Graduate School of Nanobioscience, Yokohama City University, Suehiro-cho 1-7-29, Tsurumi-ku, Yokohama 230-0045, Japan. E-mail: kawasaki@yokohama-cu.ac.jp
[3]Present address: Genome Damage and Stability Centre, University of Sussex, Falmer, Brighton, East Sussex BN1 9RQ, United Kingdom.
[4]Present address: Department of Life Science, Graduate School of Bioscience and Biotechnology, Tokyo Institute of Technology, Nagatsuda-cho 4259 B-8, Midori-ku, Yokohama 256-8501, Japan.

signaling module (Kang *et al.* 2001; Park and Bi 2007). Next, the GTPase module transmits positional information from the axial and bipolar cortical markers to the protein Cdc42p GTPase and its guanine nucleotide-exchange factor Cdc24p for polarity establishment. Finally, Cdc42p recruits the machinery that organizes and polymerizes actin, actin-associated proteins, and septins to the selected site of growth.

Numerous proteins have been found to be involved in bud-site selection (Park and Bi 2007). A genome-wide screening of homozygous deletion mutants identified 127 mutants representing three different bud-site phenotypes: unipolar, axial-like, and random (Ni and Snyder 2001). Among them, 112 mutants displayed strong or weak random budding phenotypes. The homozygous deletion mutant of the gene *BUD32* displayed a random budding pattern (Ni and Snyder 2001). *BUD32* was originally found as a gene encoding an atypical protein kinase that belongs to the piD261 family of atypical Ser/Thr protein kinases found in virtually all eukaryotic and archaeal organisms (Stocchetto *et al.* 1997). Recently, two independent studies of haploid cells have shown that Bud32p is a component of the KEOPS (*k*inase, putative *e*ndopeptidase, and *o*ther *p*roteins of *s*mall size) or the EKC (*e*ndopeptidase-like, *k*inase, *c*hromatin-associated) complexes with functions of telomere maintenance and transcriptional regulation, respectively (Downey *et al.* 2006; Kisseleva-Romanova *et al.* 2006). Cgi121p, a component of the KEOPS complex, was identified by a genome-wide screen as a suppressor of *cdc13-1*, an allele of the gene encoding the telomere-capping protein Cdc13p (Downey *et al.* 2006). The components of the KEOPS complex containing Cgi121p are the protein kinase Bud32p, the putative peptidase Kae1p, and the uncharacterized protein Gon7p. Deletion of *BUD32* or genes encoding other KEOPS components produced phenotypes with short telomeres and failed to synthesize *de novo* telomeres to DNA double-stranded breaks (Downey *et al.* 2006). The EKC complex contains a homolog of cancer-testis antigens (Pcc1p) and four additional proteins found in the KEOPS complex. Pcc1p is a transcription factor, and its deletion affects the expression of several genes regulated by α-factor and galactose (Kisseleva-Romanova *et al.* 2006). Bud32p is phosphorylated by Sch9p kinase, a yeast member of the Akt/PKB subfamily. The phosphorylation of Bud32p positively regulates its ability to interact with Grx4p and to phosphorylate it (Peggion *et al.* 2008). The signaling pathway from Akt/PKB (homolog of Sch9p) to PRPK (homolog of Bud32p) is evolutionarily conserved. Sch9p kinase regulates the nutrient signaling pathway in yeast (Roosen *et al.* 2005). The function of Bud32p in this pathway is independent of the role in the EKC/KEOPS complex (Peggion *et al.* 2008).

Genes that are specifically linked to the random budding of diploid cells encode factors important for the localization of bipolar cortical landmarks (Casamayor and Snyder 2002). Diploid cells select two poles for bipolar budding at the poles proximal or distal to the birth scar, which are determined by two cortical landmarks, Bud8p and Bud9p, respectively. *BUD8* and *BUD9* were originally identified as specific genes essential for normal bipolar budding. The *bud8*Δ and *bud9*Δ mutants bud at the proximal and distal poles, respectively (Harkins *et al.* 2001). In addition, Bud8p and Bud9p are localized at the distal and proximal poles, respectively (Harkins *et al.* 2001). Bud9p is also localized at the distal pole, whose localization may inhibit the function of Bud8p through an interaction between the two (Taheri *et al.* 2000). Previous study suggests that many of the genes that specifically cause random budding, when deleted, are associated with the localization of Bud8p (Ni and Snyder 2001). Rax1p and Rax2p are interdependently related in the maintenance of bipolar budding (Kang *et al.* 2004). The genes encoding these proteins were identified by screening genes that restored bipolar budding patterns in the haploid *axl1*Δ mutant (Fujita *et al.* 1994). Bud8p and Bud9p interact with and depend on Rax1p and Rax2p, respectively, for their localization (Kang *et al.* 2004). The delivery of Bud8p and Bud9p to the presumptive bud site and mother-bud neck, respectively, is dependent on actin. The delivery of Bud9p is also dependent on septin (Schenkman *et al.* 2002).

In this article, we report that the Sch9p kinase cascade does not associate with bipolar budding, but that the EKC/KEOPS complex is involved in bipolar budding. The deletion mutants of each EKC/KOEPS component displayed a random budding pattern, and the phenotype was suppressed by the deletion of *BUD9*, suggesting that Bud9p is a cause of random budding in these mutants. Consistent with phenotypic analysis, the asymmetric localization of GFP-Bud9p was dependent on the EKC/KEOPS complex, but GFP-Bud8p was not. The localization of Bud9p is also regulated interdependently by Rax1p/Rax2p. The phenotype of double mutants of each *EKC/KEOPS* gene and *RAX2* was changed to one similar to the *rax2*Δ mutant, which showed a random budding pattern specifically in diploid cells. The localization of Rax2p was normal even in *bud32*Δ and other mutant cells with deleted EKC/KEOPS components. These results suggest that the EKC/KEOPS complex is required for the localization of Bud9p and acts as a downstream factor of Rax2p.

Materials and Methods

Yeast strains, culture medium, plasmids, and recombinant DNA methods

Homozygous deletion mutants were generated by mating *MAT***a** cells with *MAT*α cells or by transformation of the plasmid expressing the HO (Homothallic switching) endonuclease in haploid cells, which is expected to cause mating-type switching of *MAT***a** cells to *MAT*α or *MAT*α cells to *MAT***a** and hence subsequent mating between *MAT***a** and *MAT*α cells to form a homozygous diploid. In the supporting information, Table S1 summarizes the yeast strains used in this study. Yeast cells were grown in yeast extract peptone dextrose [YPD: 2% (w/v) bacto-peptone, 1% (w/v) yeast extract, and 2% (w/v) glucose] or in synthetic defined

(SD) medium [0.2% (w/v) yeast nitrogen base without amino acids and ammonium sulfate, 0.5% (w/v) ammonium sulfate, and 2% (w/v) glucose] or in synthetic complete (SC) medium [0.2% (w/v) yeast nitrogen base without amino acids and ammonium sulfate, 0.5% (w/v) ammonium sulfate, 2% (w/v) glucose, and complete amino acids] lacking appropriate amino acids to maintain various plasmids. Plasmid preparation was conducted with *Escherichia coli* XL10 GOLD (Stratagene, La Jolla, CA) grown in Luria–Bertani medium [0.5% (w/v) NaCl, 1% (w/v) yeast extract, and 1% (w/v) tryptone] containing 50 $\mu g \cdot ml^{-1}$ ampicillin. Solid media were made with 2% agar. Table S2 summarizes the plasmids used in this study. Standard methods of yeast genetics and DNA manipulation (Gietz *et al.* 1992; Ausubel *et al.* 1995; Longtine *et al.* 1998) were used, except where noted. Polymerase chain reaction (PCR) was performed using KOD FX DNA polymerase (Nacalai Tesque, Kyoto, Japan). Oligonucleotide primers shown in Table S3 were synthesized and purchased from Invitrogen (Tokyo).

Plasmids

The pYC01 was created with pRS425 (Christianson *et al.* 1992) by inserting a fragment containing an upstream sequence of 808 bp, an open reading frame of *BUD8*, and a downstream sequence of 517 bp. PCR was performed to amplify the *BUD8* region with the primer set BUD8a/BUD8b and the genomic DNA of the BY4743 yeast strain as a template. The resulting *Xho*I/*Spe*I fragment was cloned into *Xho*I/*Spe*I-digested pRS425. Detailed procedures for the preparation of pYC03 to insert epitope tags using a *Mlu*I cleavable site (5′-ACGCGT-3′) just downstream of the start codon of *BUD8* have been reported (Kato *et al.* 2009). For green fluorescent protein (GFP) tagging, PCR was performed using the primer set GFPa/GFPb and pFA6a-GFP^{S65T}-kanMX6 (Longtine *et al.* 1998) as a template. The resulting *Mlu*I fragment was incubated with T4 polynucleotide kinase (T4 PNK) (Takara Shuzo, Kyoto, Japan) and then ligated with *Eco*RV-digested pBluescript (SK–) to create pYC05. *Mlu*I-digested pYC05 was separated using 1.5% agarose gel electrophoresis and gel-extracted. The resulting insert was ligated with *Mlu*I-digested pYC03 to generate pYC14. The GFP-Bud9p fragment was cloned into pRS426 (Christianson *et al.* 1992) using the same procedure to generate the pYC06.

The pYC09 was constructed to delete *GON7*. PCR was first performed to amplify the GON7 region with the primer set GON7a/GON7b, with genomic DNA of the BY4743 yeast strain as the template. The resulting fragment containing an upstream 570 bp, an open reading frame of *GON7*, and a downstream 519 bp was phosphorylated with T4 PNK and then cloned in *Eco*RV-digested pBluescript (SK–) to create pYC07. Deletion of the open reading frame of *GON7* and creation of a *MluI* restriction site to generate pYC08 were performed by PCR using the primer set GON7c/GON7d and pYC07 as a template. For cloning the *URA3* region as a selective marker, PCR was next performed using the primer set URA3a/URA3b and genomic DNA of the B8032 strain as the template. The resulting *Mlu*I fragment containing an upstream 871 bp, an open reading frame of *URA3*, and a downstream 1000 bp was digested with *Mlu*I and then cloned into *Mlu*I-digested pYC08 to create pYC09.

For FLAG tagging, PCR was performed using a primer set, FLAGa/FLAGb, and pTM55 as the template. The resulting fragment was digested with *Mlu*I and then ligated with *Mlu*I-digested pYC04 to create pYC10.

The pYC11 was created with pBluescript (SK−) by inserting a fragment containing an upstream sequence of 520 bp, an open reading frame of *BUD32*, and a downstream sequence of 789 bp. PCR was performed to amplify the *BUD32* region with the primer set BUD32a/BUD32b and the genomic DNA of the BY4743 yeast strain as a template. The resulting *Spe*I/*Xho*I fragment was cloned into *Spe*I/*Xho*I-digested pBluescript (SK−) to generate pYC11. Site-directed mutagenesis was performed to insert a *Mlu*I cleavable site (5′-ACGCGT-3′) just upstream of the stop codon of *BUD32* with primer set BUD32c/BUD32d and pYC11 as a template to generate pYC12.

Plasmids pYC13 and pYC15 were created with pBluescript (SK−) by replacing base pairs of *BUD32* to mutate to alanine at Lys52 and Ser258 of Bud32p, respectively. PCR was performed to replace base pairs with the primer sets BUD32e/BUD32f, BUD32g/BUD32h, and pYC12 as a template to generate pYC13 and pYC15, respectively. The pYC13 was then digested with *Spe*I/*Xho*I, and the insert of pYC13 was transferred to pRS306 to generate pYC16.

*Mlu*I-digested pYC05 was separated using 1.5% agarose gel electrophoresis and gel-extracted. The resulting insert was ligated with *Mlu*I-digested pYC12, pYC13, and pYC15 to generate pYC17, pYC18, and pYC19, respectively. The resulting plasmids were then digested with *Spe*I/*Xho*I, and the inserts of these plasmids were transferred to pRS306 to generate pYC20, pYC21 and pYC22, respectively. All sequences were verified using an ABI 3010 sequencer (Applied Biosystems, Foster City, CA).

Strains

Strains expressing Rax2p-GFP, CCY032, and CCY033 were created by a one-step tagging method using PCR product (Longtine *et al.* 1998). A cassette of GFP^{S65T}-kanMX6 just upstream of the stop codon of *RAX2* using the primer set RAX2-GFPa/RAX2-GFPb and pFA6a-GFP^{S65T}-kanMX6 as a template was amplified by PCR. The BY4741 and BY4742 strains were transformed with the resulting fragments to create strains CCY032 and CCY033, respectively. The transformants were incubated on YPD plates at 30° for 1 day and then selected to YPD plates with G418 (100 $\mu g \cdot ml^{-1}$). The correct insertion of GFP^{S65T}-kanMX6 was verified by PCR using the genomic DNA of candidates as the template. The haploid strains CCY032 and CCY033 were mated on YPD plates for 1 day at 30° and then selected on SC plates not containing Lys and Met for 2 days at 30° to obtain the diploid strain expressing Rax2p-GFP (CCY034).

The *GON7* deletion strains (CCY015, CCY016, CCY 022, and CCY025) were created by homologous recombination with PCR products from pYC09. PCR was performed using the primer set GON7a/GON7b and pYC09 as the template. The resulting fragment was transformed in *bud32*Δ (CCY001), *cgi121*Δ (CCY004), *bud8*Δ (CCY010), and *bud9*Δ (CCY012) mutants, respectively, and then the transformants were grown on SC−Ura for 3 days at 25°. Alternatively, the one-step disruption method using PCR products was used to delete *GON7* in RAX2-GFP (CCY034) or *rax2*Δ (CCY044) strains. PCR was performed using the primer set GON7e/GON7f and pFA6a-His3MX6 as the template. The resulting fragment was transformed in the diploid strains CCY034 and CCY044, and then the transformants were grown in SC−His at 25° for 3 days. The resulting heterozygous strains CCY039 and CCY049 were then confirmed by PCR using these genomic DNAs as templates to verify disruption of *GON7*. After dissection and selection of spores from these strains, PCR was used to confirm the deletion of *GON7* and *RAX2* using genomic DNA of these segregates as the template to obtain the haploid strains CCY040 and CCY050, respectively. *MAT***a** or *MAT*α was identified by mating with reference strains on SD plates for 3 days at 25°.

The strain expressing Bud32p-GFP (CCY052) was created by homologous recombination with a linearized fragment of pYC20, respectively. The pYC20 fragment was digested with *Sph*I and purified by a gel extraction. The resulting linearized fragments were transformed in BY4741 strain. Transformants were incubated on YPD plate at 25° for 3 days and then transferred to an SC plate with 5-FOA (1 mg·ml^{-1}) at 25° for 3 days. After the single isolation of colonies on YPD plate, the resulting strain (CCY052) was confirmed by PCR using these genomic DNAs as templates to verify the correct insertion of *BUD32-GFP*. The diploid *BUD32-GFP* strain (CCY053) was generated by transformation of the plasmid expressing the HO endonuclease in the CCY052 strain. The growth rate of the resulting strain (CCY053) was confirmed to be identical to that of the BY4743 strain by a spotting assay.

Strains expressing Bud32p (K52A) (CCY064), Bud32p (K52A)-GFP (CCY054 and CCY055), and Bud32p (S258A)-GFP (CCY067) were created by homologous recombination with a linearized fragment of pYC16, pYC21, and pYC22, respectively, using the same procedure to generate CCY052. The diploid *bud32 (K52A)-GFP* strain (CCY056) was generated by mating CCY054 with CCY055, and the diploid *bud32 (S258A)-GFP* strain (CCY068) was generated by transformation of the plasmid expressing the HO endonuclease in CCY067.

Strains expressing Bud32p-13myc (CCY062) and Bud32p (K52A)-13myc (CCY065) were created by the one-step tagging method using PCR product (Longtine *et al.* 1998). A cassette of 13Myc-kanMX6 just upstream of the stop codon of *BUD32* using the primer set BUD32i/BUD32j and pFA6a-13Myc-kanMX6 as a template was amplified by PCR. The BY4741 and CCY064 strains were transformed with the resulting fragment to generate strains CCY062 and CCY065, respectively. The transformants were incubated on YPD plates at 30° for 1 day and then selected to YPD plates with G418 (100 μg·ml^{-1}). The correct insertion of 13Myc-kanMX6 was verified by PCR using genomic DNA of candidates as the template. Diploid strains (CCY063 and CCY066) were generated by transformation of the plasmid expressing the HO endonuclease in CCY062 and CCY065, respectively. The growth rate of resulting the strain (CCY063) was confirmed to be identical to that of the BY4743 strain by the spotting assay.

Strains expressing Cdc11p-GFP (CCY071 and CCY072) were created by the one-step tagging method using PCR product (Longtine *et al.* 1998). A cassette of GFP^{S65T}-kanMX6 just upstream of the stop codon of *CDC11* using the primer set CDC11a/CDC11b and pFA6a-GFP^{S65T}-kanMX6 as a template was amplified by PCR. The BY4741 and BY4742 strains were transformed with the resulting fragments to generate strains CCY071 and CCY072, respectively. The transformants were incubated on YPD plates at 30°C for 1 day, and then selected to YPD plates with G418 (100 μg·ml^{-1}). The correct insertion of GFP^{S65T}-kanMX6 was verified by PCR using genomic DNA of candidates as the template. Diploid strain (CCY073) was generated by mating CCY071 with CCY072. The growth rate of resulting strain (CCY073) was confirmed to be identical to that of BY4743 strain by a spotting assay.

Analysis of budding patterns

Cells grown to late log phase were harvested by centrifugation at 3000 × *g* for 5 min, washed twice, and resuspended in water. Cells were fixed with a paraformaldehyde solution to a final concentration of 3.7% with gentle agitation for 30 min at room temperature. The fixed cells were washed twice and resuspended in water and then incubated with a final concentration of 5 μg·ml^{-1} calcofluor white for 20 min to visualize bud and birth scars. After washing twice with water, the fluorescent image of chitin rings was observed with an ECLIPSE 80ι fluorescence microscope (Nikon, Tokyo) using a UV filter set.

Budding patterns were analyzed according to Chen *et al.* (2000). All analyses were performed in homozygous diploids. The bud-scar positions of daughter and mother cells were separately counted and analyzed. The daughter cells with the first bud scar were classified in relation to the bud position to the birth scar as "proximal" when one bud scar was at the proximal pole, as "distal" when one bud scar was at the distal pole, or as "random" when one bud scar was around equatorial region. The mother cells that had more than three bud scars were used (Chant and Pringle 1995) and classified on the basis of the relation of the bud positions to the birth scar as "bipolar" when one or more bud scars were at both poles, as "proximal" when all bud scars were at the proximal pole, as "distal" when all bud scars were at the distal pole, as "axial-like" when all bud scars were connected in a chain with at least one touching the birth scar, or as "random" when at least one or more bud scars were in the

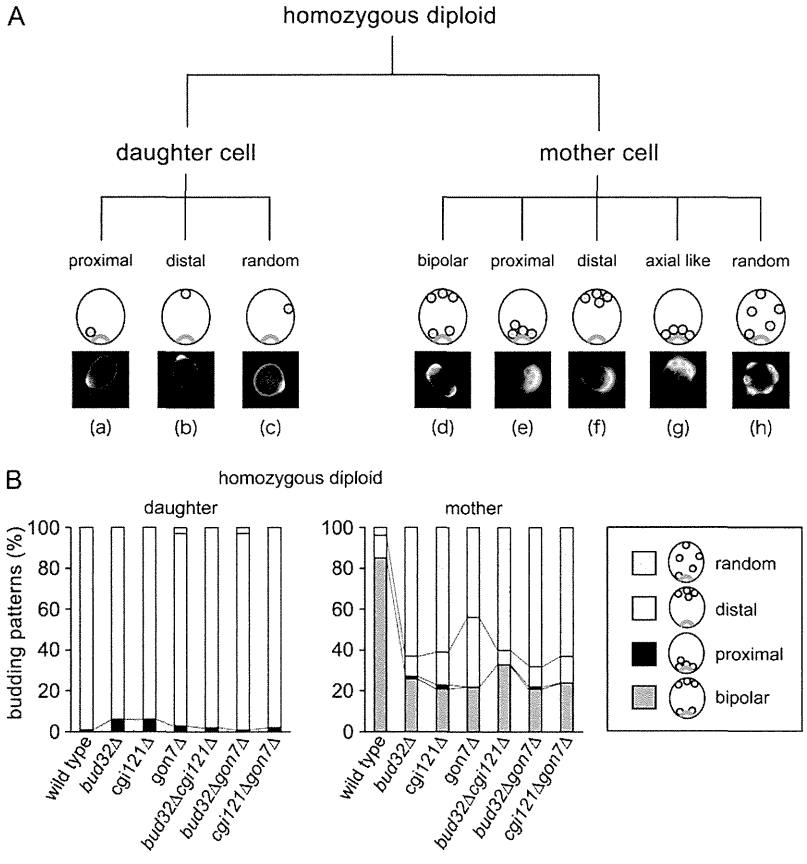

Figure 1 Budding pattern of the deletion mutants of each EKC/KEOPS component in diploid cells. (A) Representative image of budding patterns in both diploid daughter and mother cells. Daughter cells showed three budding patterns in the wild type and mutants. The positions of the first buds on diploid daughter cells were scored as being at the pole proximal to the birth scar (a), at the pole distal to the birth scar (b), or at a random site (c) on the cell. Mother cells showed five budding patterns in the wild type and mutants. Each diploid mother cell budding pattern was determined by counting cells with more than three bud scars. Bud scars were concentrated at the two poles (d, as bipolar), only at the pole proximal [e and g (as chain-like bud)] or distal (f) to the birth scar, and at the random sites (h). (B) Budding patterns of the diploid deletion mutants. Strains used were diploid wild type (BY4743) and *bud32Δ* (CCY003), *cgi121Δ* (CCY006), *gon7Δ* (CCY009), *bud32Δcgi121Δ* (CCY017), *bud32Δgon7Δ* (CCY018), and *cgi121Δgon7Δ* (CCY019). Budding positions are classified as in the budding patterns of diploid cells in Figure 1A. At least 150 cells were scored for each bud scar pattern from both daughter and mother cells (the percentages are indicated). In daughter cells, the solid, open, and dotted boxes indicate cells with buds at only the proximal pole, at only the distal pole, and at a random site, respectively. In mother cells, the shaded, solid, open, slashed, and dotted boxes indicate cells with buds at two poles, at only the proximal pole, at only the distal pole, at the axial-like, and at random sites, respectively.

equatorial region. A representative image of each pattern in both daughter and mother cells is shown in Figure 1A. Over 150 cells of each mother and daughter cell were counted for the classification. For each strain, the average value from two independent experiments is shown.

Fluorescence microscopy

Cells expressing GFP-fused protein were grown for 12–16 h at 25° and then harvested by centrifugation at 3000 × *g* for 5 min, stained with calcofluor white, washed twice, and resuspended in water. The fluorescent images of the GFP-fused proteins and bud scars in cells were observed under a fluorescence microscope (BZ-9000; Keyence, Osaka, Japan) using GFP and UV filter sets, respectively.

Western blotting

Yeast cell lysates were prepared as previously reported (Krappmann *et al.* 2007). Briefly, the same OD_{600} units of cells were resuspended in an 80-μl extraction buffer [50 mM Tris–HCl (pH 7.5), 50 mM DTT, 1 mM EDTA, and inhibitor cocktail; Roche, Basel, Switzerland], vortexed with glass beads for 10 min at 4° followed by an additional 20 μl of membrane extraction buffer [50 mM Tris–HCl (pH 7.5), 50 mM DTT, 1 mM EDTA, 10% SDS, and 5% Triton X-100] and then vortexed at 4° for 1 min. The protein concentration of the resulting extracts was determined by the Bradford method (Kruger 1994). Proteins were subjected to SDS-PAGE with 15% low-bis gels (Hirano 1989). The separated proteins were electroblotted onto polyvinylidene fluoride membranes as described in Hirano (1989). Membrane blocking was performed using the method of Kawasaki *et al.* (2008). Monoclonal mouse anti-FLAG (Sigma-Aldrich, St. Louis) and peroxidase-coupled goat anti-mouse immunoglobulin G (Santa Cruz Biotechnology, Santa Cruz, CA) were used as primary and secondary antibodies, respectively.

Results

Complex made with Bud32p, Cgi121p, and Gon7p regulates bipolar bud-site selection

The EKC/KEOPS complex consists of Kae1p, Bud32p, Cgi121p, Gon7p, and Pcc1p in haploid cells (Downey *et al.* 2006; Kisseleva-Romanova *et al.* 2006). We investigated whether the EKC/KEOPS complex is involved in bipolar bud-site selection. By using tandem affinity purification (TAP), we confirmed that the components of the complex pulled down with Bud32p-TAP or Gon7p-TAP from diploid cells are the same as those of the haploid EKC/KEOPS complex (Y. Kato, H. Kawasaki, and H. Hirano, unpublished results). The budding patterns of the deletion mutants of each EKC/KEOPS component were analyzed, except those of *KAE1* and *PCC1*, whose deletion showed a severe growth defect. The budding patterns of diploid cells were classified as shown in Figure 1A. The first buds in daughter diploid cells of these mutants were at the distal pole, as observed in

Table 1 Budding patterns of homozygous diploid strains

	Budding = 1			Budding > 3				
	Proximal	Distal	Random	Bipolar	Proximal	Distal	Random	Axial-like
BY4743	1	99	0	85	0	11	4	0
bud32Δ	6	94	0	26	1	10	63	0
cgi121Δ	6	94	0	21	2	16	61	0
gon7Δ	3	94	3	22	0	34	44	0
bud32Δ cgi121Δ	2	98	0	33	0	7	60	0
bud32Δ gon7Δ	1	98	1	21	1	10	68	0
cgi121Δ gon7Δ	4	96	0	24	0	13	63	0
bud8Δ	95	0	5	5	95	0	0	0
bud9Δ	0	99	1	0	2	98	0	0
bud32Δbud8Δ	67	18	15	29	28	2	41	0
cgi121Δbud8Δ	53	30	17	28	15	0	57	0
gon7Δbud8Δ	96	2	2	13	86	0	1	0
bud32Δbud9Δ	5	95	0	20	2	69	9	0
cgi121Δbud9Δ	<1	99	<1	23	1	66	10	0
gon7Δbud9Δ	<1	99	<1	16	0	81	3	0
rax2Δ	52	33	15	17	2	1	65	15
bud32Δ rax2Δ	51	35	14	18	1	0	70	11
cgi121Δ rax2Δ	50	37	13	22	0	1	66	11
gon7Δ rax2Δ	50	36	14	20	0	0	68	12
K52A	2	96	2	36	0	11	53	0
K52Abud8Δ	76	6	18	29	14	1	56	0
K52Abud9Δ	8	92	0	14	1	74	11	0
sch9Δ	3	97	0	91	1	4	4	0
S258A	3	96	1	85	0	11	4	0

Each value indicates the percentage of total cells.

the wild-type diploid cells (Figure 1B). The deletion of each component of the EKC/KEOPS complex did not affect the budding pattern of daughter diploid cells, while the mother diploid cells of these mutants showed a severe budding defect (Figure 1B and Table 1). About half of the mother cells showed a random budding pattern in these mutants, although the *gon7Δ* mutant displayed a slightly different phenotype with a higher distal budding ratio. We also examined the phenotype of several double mutants, in which two genes of the complex component were disrupted. The phenotypes of *bud32Δcgi121Δ*, *bud32Δgon7Δ*, and *cgi121Δgon7Δ* double mutants were very similar to those of the single mutants. (Figure 1B and Table 1). These results suggest that *BUD32*, *CGI121*, and *GON7* act in the same process as a complex.

Random budding of bud32Δ, cgi121Δ, and gon7Δ is suppressed by deletion of BUD9 but not BUD8

Bud8p and Bud9p are cortical landmarks in diploid cells for the distal and proximal poles, respectively (Harkins *et al.* 2001), because each deletion of these landmarks displays unipolar budding at the distal or the proximal pole, respectively. The first buds of daughter cells in *bud32Δ*, *cgi121Δ*, or *gon7Δ* mutants formed at the distal pole as in wild-type cells (Figure 1B and Table 1). This indicates that Bud32p, Cgi121p, and Gon7p may not be related to marking of the distal pole with Bud8p. We observed the effect of the deletion of *BUD8* or *BUD9* in the *bud32Δ*, *cgi121Δ*, and *gon7Δ* mutant cells. In the daughter cells of the *bud32Δbud8Δ* double mutant, the buds were observed largely at the proximal pole (~60%), but some were at the distal pole (20%) and at the equatorial sites (~20%) (Figure 2A and Table 1). The budding pattern of daughter cells in the *cgi121Δbud8Δ* double mutant was similar to that of the *bud32Δbud8Δ* double mutant. In contrast, that of daughter cells in the *gon7Δbud8Δ* double mutant was similar to that of the *bud8Δ* mutant in that the first bud of >90% of cells shows the proximal budding. Because the proximal budding observed in the *bud8Δ* mutant would be dependent on Bud9p, Bud9p seems to act as the proximal marker in daughter cells of these double mutants. However, ~30–50% of cells in *bud32Δbud8Δ* and *cgi121Δbud8Δ* mutants budded at the distal pole or at the equatorial site. Thus, the proximal marker may be somewhat impaired in these mutants.

In the *bud32Δbud9Δ* double mutant, the first and subsequent buds were formed at the distal pole, as in the *bud9Δ* mutant (Figure 2A and Table 1). Similar results were obtained for the *cgi121Δbud9Δ* and *gon7Δbud9Δ* double mutants. Because distal budding of the *bud9Δ* mutant would be dependent on Bud8p, these observations suggest that Bud8p in daughter cells of these mutants still acts as the distal landmark.

As shown in Figure 1B, ~45–60% of *bud32Δ*, *cgi121Δ*, and *gon7Δ* mutant mother cells showed a random budding pattern. Similarly, ~40–60% of *bud32Δbud8Δ* and *cgi121Δbud8Δ* double-mutant mother cells showed a random budding pattern (Figure 2B). A distal budding pattern, which was observed in ~15% of *bud32Δ*, *cgi121Δ*, and *gon7Δ* mutant cells, was almost completely suppressed and replaced with a proximal budding pattern (Figure 1B and Figure 2B). However, the majority of the double mutants showed a random budding pattern, although the ratio of the proximal budding pattern increased slightly.

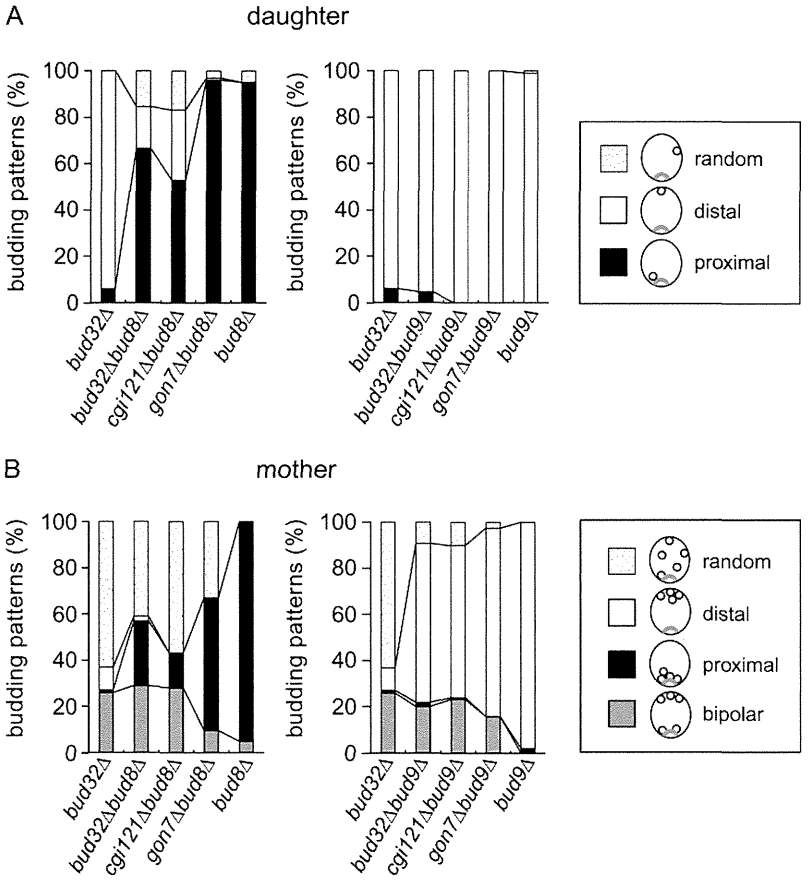

Figure 2 Genetic interaction between *BUD8* or *BUD9* and *EKC/KEOPS* genes. (A and B) Budding pattern of daughter (A) and mother (B) cells with *BUD8* or *BUD9* deletion in the *bud32Δ*, *cgi121Δ*, and *gon7Δ* mutant backgrounds. Strains used were the diploid wild type (BY4743), *bud8Δ* (CCY011), *bud9Δ* (CCY013), *bud32Δ* (CCY003), *bud32Δbud8Δ* (CCY026), *cgi121Δbud8Δ* (CCY027), *gon7Δbud8Δ* (CCY028), *bud32Δbud9Δ* (CCY029), *cgi121Δbud9Δ* (CCY030), and *gon7Δbud9Δ* (CCY031). Budding positions are classified as in the budding pattern of diploid cells in Figure 1A. At least 150 cells were scored for each bud scar pattern from both daughter and mother cells (the percentages are indicated). The solid, open, and dotted boxes in A indicate daughter cells budded at proximal, distal, and equatorial sites, respectively. The shaded, solid, open, and dotted boxes in B indicate mother cells with buds at two poles, at only the proximal pole, at only the distal pole, and at the random site, respectively.

In mother cells of *bud32Δbud9Δ* double mutants, the random budding pattern was replaced by a distal budding pattern, although bipolar budding observed in the *bud32Δ* mutant was still seen in the double mutant (Figure 2B and Table 1). The random budding of mother cells of *cgi121Δ* and *gon7Δ* mutants was also suppressed by *BUD9* deletion. In the absence of Bud9p, a random budding pattern clearly replaced the distal budding pattern in which Bud8p was marked at the distal pole. These results suggest that the proximal marking by Bud9p is regulated by Bud32p and other components of the EKC/KEOPS complex.

Localization of the bipolar landmarks Bud8p and Bud9p

We showed that *BUD9*, but not *BUD8*, is required for random budding of *bud32Δ*, *cgi121Δ*, and *gon7Δ* mutants. Therefore, we observed the localization of these bipolar landmarks in the wild type, and these mutant cells in GFP-tagged Bud8p or Bud9p expressed with a high-copy vector with fluorescence microscopy. The expression of GFP-Bud8p or GFP-Bud9p in diploid *bud8Δ* or *bud9Δ* mutant cells complemented the budding defects, suggesting that these tagged proteins provide a normal function. In the wild-type cells, GFP-Bud8p was localized at the distal pole in 36% of unbudded cells (n = 439) and at the proximal pole in 17% of such cells (Figure 3A, cells 1 and 2, and Table 2). The GFP-Bud8p signal in mother cells appeared to be weaker than that in daughter cells. It was localized at the bud tip in 17% of small-/large-budded cells (n = 529) and at the bud tip/neck in 22% of such cells (Figure 3A, cells 3–7, and Table 2). Localization only to the bud neck was also observed in 7% of such cells (Figure 3A, cell 8, and Table 2). GFP-Bud9p was localized at the proximal pole in 17% of unbudded cells (n = 200), and the signal at the distal pole was observed in only 5% of such wild-type mother cells (Figure 3B, cells 1 and 2, and Table 3). In addition, GFP-Bud9p was also localized at the proximal pole (10%), bud neck (7%), and bud neck/proximal pole (9%) in small-/large-budded cells (n = 254; Figure 3B, cells 3–8, and Table 3).

In the *bud32Δ*, *cgi121Δ*, and *gon7Δ* mutants, the localization patterns of GFP-Bud8p were essentially identical to that of the wild type, but its GFP signal appeared to be very diffused around the poles, tips, and bud necks (Figure 3C, cells 1–5, and Table 2; GFP-Bud8p localization patterns in the *cgi121Δ* mutant are those of the representative mutant). In addition, GFP-Bud8p was also observed at the bud tip and bud neck in cells that had bud scars at the equatorial position (Figure 3C, cells 5–8).

However, the localization to both poles and the bud neck of the GFP-Bud9p signal dramatically decreased compared to those of the wild-type cells (~3% of all cells) (Table 3). No GFP signal was observed in most cells (Figure 3D, cells 1–4; localization patterns of GFP-Bud9p in the *cgi121Δ* mutant are those of the representative mutant), but a few cells were also present with the GFP signal in which normal

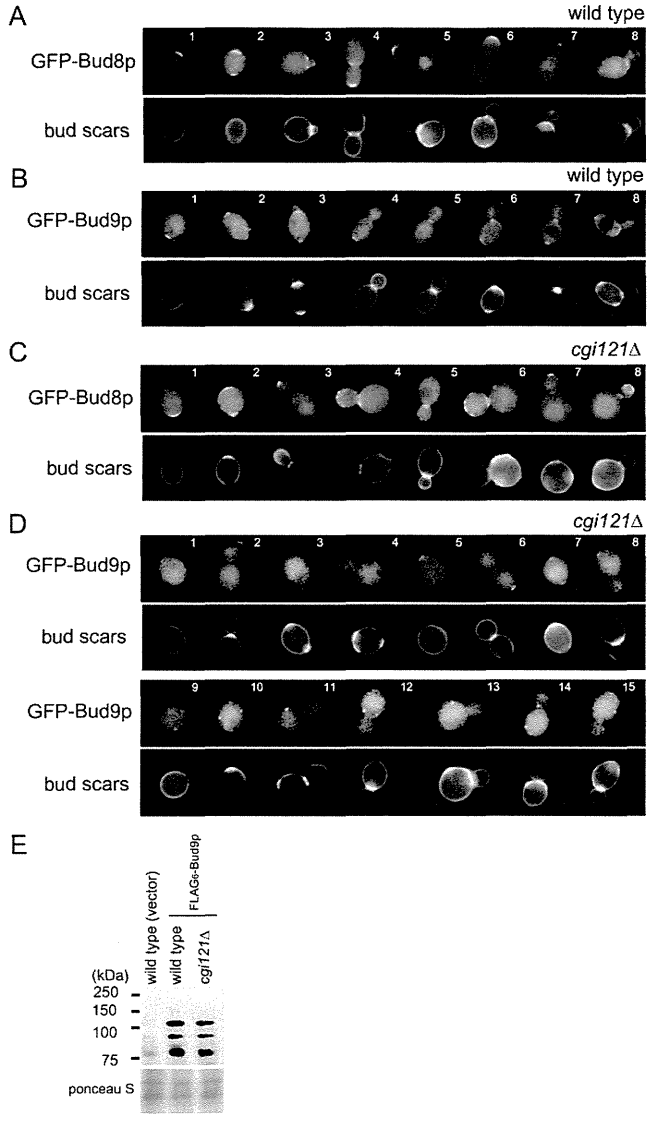

Figure 3 Effect on the localization of GFP-Bud8p and GFP-Bud9p due to loss of EKC/KEOPS components. (A and B) Localization patterns of GFP-Bud8p and GFP-Bud9p in the wild type. Wild type (BY4743) expressing the full-length GFP-Bud8p or GFP-Bud9p from its own promoter in pYC14 or pYC06, respectively, was grown for 12–16 h at 25° in synthetic complete (SC)−Leu or −Ura liquid medium, stained with calcofluor white, and then suspended in water for observation. GFP-Bud8p or GFP-Bud9p and bud scars were observed with a fluorescence microscope with GFP and UV filter sets, respectively. (C and D) Localization of GFP-Bud8p and GFP-Bud9p in the *cgi121Δ* mutant. The *cgi121Δ* (CCY006) expressing full-length GFP-Bud8p or GFP-Bud9p from their own promoters in pYC14 or pYC06 was grown for 12–16 h at 25° in SC−Leu or −Ura liquid medium, stained with calcofluor white, and then suspended in water for observation. GFP-Bud8p or GFP-Bud9p and bud scars were observed with a fluorescence microscope with GFP and UV filter sets, respectively. (E) Expression level of Bud9p in the absence of Cgi121p. Diploid wild type (BY4743) and *cgi121Δ* mutant (CCY006), both expressing the $FLAG_6$-Bud9p in pYC10, were analyzed by Western blotting. The wild type (BY4743) was considered the control, which carried the empty pRS426. Cells were grown overnight to log phase in SC medium lacking uracil. The total cell extract from the same OD_{600} units of cells was analyzed by immunoblotting using an anti-FLAG antibody (top) and stained with Ponceau-S as a loading control (bottom).

Bud9p localization was observed (Figure 3D, cells 5–8, and Table 3). Another visible GFP signal was observed primarily as a dot-like structure along the cell periphery of both daughter and mother cells (Figure 3D, cells 9–15). Because no obvious difference was seen at the *BUD9* expression levels of mRNA and protein between the wild-type and mutant cells, we concluded that mislocalization of the GFP signal in these mutants was not due to a difference in Bud9p expression (Figure 3E and real-time PCR; Y. Kato, H. Kawsaki, and H. Hirano, unpublished data). These results also suggest that Bud32p, Cgi121p, and Gon7p are specifically related in the localization of Bud9p, but not Bud8p.

Bud32p kinase activity is required for Bud9p localization

We generated a kinase dead mutant (*bud32-K52A*) by replacing the 52nd lysine residue with alanine in Bud32p, which is the binding site for the α- and β-phosphates of ATP (Mao *et al.* 2008), to investigate whether kinase activity is required for the regulation of bipolar bud-site selection. The mutant displayed a random budding pattern, as observed in the *bud32Δ* mutant (Figure S1A and Table 1). These results suggest that kinase activity is also required for regulation of bipolar bud-site selection. We observed the effect of deleting *BUD8* or *BUD9* in the kinase dead mutant (*bud32-K52A*); the deletion of *BUD9* suppressed random budding in the kinase dead mutant, but deletion of *BUD8* did not (Figure S1, B and C, and Table 1). Finally, we examined the localization of GFP-Bud8p and GFP-Bud9p in the mutant (Figure S1D). In the kinase dead mutant, the GFP-Bud8p localization pattern was similar to that of wild-type cells, whereas the GFP-Bud9p signal was not observed in the kinase dead mutant, as in the *bud32Δ* mutant (Figure S1D). These results indicate that kinase activity is required for proper localization of Bud9p, but not Bud8p.

Mutation at Ser258 of Bud32p did not affect bipolar bud-site selection

A recent report has suggested that Bud32p is involved in the Sch9p signaling pathway (Peggion *et al.* 2008). We investigated whether this signaling pathway is involved in bipolar bud-site selection. Sch9p, a homolog of yeast Akt, phosphorylates Bud32p at Ser258. This phosphorylation of Bud32p positively regulates its ability to interact with Grx4p and to phosphorylate it. We constructed a mutant *bud32-S258A* in which Ser258 on Bud32p was replaced with Ala. We observed the budding patterns of *sch9Δ* and *bud32-S258A*. The budding patterns of these two mutants were similar to those of wild-type daughter and mother cells (Figure S2 and Table 1). This result suggests that the Sch9p signaling cascade is not related to bipolar bud-site selection.

Genetic interaction between RAX2 and EKC/KEOPS genes

Rax1p and Rax2p are interdependently localized and also involved in Bud9p localization via interactions (Kang *et al.* 2004). In daughter cells of the *rax2Δ* mutant, about half of the first buds were at the distal pole, and the rest were at the

Table 2 Localization patterns of GFP-Bud8p

	Unbudded cells			Budded cells				
	Distal	Both poles	No signal	Bud tip	Bud neck	Bud tip/neck	No signal	Others
BY4743	19	17	64	17	7	22	59	5
bud32Δ	20	10	70	20	6	20	51	3
cgi121Δ	15	14	71	15	6	29	46	4
gon7Δ	17	19	64	19	10	25	49	7

Each value indicates the percentage of total cells.

proximal pole. Mother cells of *rax2Δ* mutants largely showed a random budding pattern, as in the *bud32Δ*, *cgi121Δ*, and *gon7Δ* mutants. However, the phenotype differed between *rax2Δ* and EKC/KEOPS mutants although the ratio of random budding in both mutants was almost the same. A small number of *rax2Δ* mutant cells showed axial-like budding, while a few *bud32Δ* mutant cells showed distal budding (Figure 4A). We deleted *RAX2* in the *bud32Δ*, *cgi121Δ*, and *gon7Δ* mutant cells and observed the budding pattern of these mutants (Figure 4A). In both daughter and mother cells of the double mutants, the phenotype was changed to one similar to the *rax2Δ* mutant (Figure 4A and Table 1). The distal budding pattern of the *bud32Δ* mutant disappeared following *RAX2* deletion and was replaced with an axial-like budding pattern. The axial budding pattern was never observed in the single mutants *bud32Δ*, *cgi121Δ*, and *gon7Δ*.

We observed Rax2p-GFP in wild-type and mutant cells (Figure 4, B and C, and Figure S3). Cells chromosomally expressing Rax2p-GFP also displayed a bipolar budding pattern, as in wild-type cells, suggesting that Rax2p-GFP is functional. In wild-type cells, Rax2p-GFP localized mainly to bud scars and birth scars in unbudded cells and sometimes to bud tips in budded cells. Similar results were obtained from *bud32Δ*, *cgi121Δ*, and *gon7Δ* single mutants (Figure 4B and Figure S3A). In addition, the localization of Rax2p at bud scars could be observed even in equatorial bud scars, suggesting that the regulation for localization of Rax2p is normal in the mutants (Figure 4C and Figure S3B).

Discussion

EKC/KEOPS complex is required for bipolar bud-site selection

BUD32 was originally found as a gene encoding an atypical protein kinase found in virtually all eukaryotic and archaeal organisms (Stocchetto *et al.* 1997). It was also identified as a gene that regulates bud-site selection of diploid cells through a genome-wide analysis (Ni and Snyder 2001). Bud32p is involved in the signaling pathway of Sch9p kinase (Peggion *et al.* 2008) and is also involved in telomere or transcriptional regulation as a component of the EKC/KEOPS complex (Downey *et al.* 2006; Kisseleva-Romanova *et al.* 2006). In an analysis with gel-filtration chromatography in haploid cells, the subcomplex containing only Kae1p and Bud32p was observed in yeast cells although it could have been a preparation artifact (Kisseleva-Romanova *et al.* 2006). No other subcomplex has been reported. We purified the EKC/KEOPS complex from diploid cells using a TAP pull-down. The diploid EKC/KEOPS complex was composed of Bud32p, Cgi121p, Kae1p, Gon7p, and Pcc1p, which is identical to the haploid complex. Of the genes encoding these components, *CGI121* and *GON7* were identified as new genes required for bipolar bud-site selection (Figure 1B). The EKC/KEOPS complex regulates bipolar bud-site selection, as deletion of the components showed a very similar phenotype with random budding. We also revealed that the kinase activity of Bud32p is required for bipolar bud-site selection (Figure S1). This activity is essential for the functions of the EKC/KEOPS complex, such as transcriptional regulation and telomere maintenance, and it is also contributed to, but was not absolutely essential for, the Sch9p signaling cascade (Peggion *et al.* 2008). In addition, we observed that phosphorylation at Ser258 on Bud32p by Sch9p, the modification of which did not alter its kinase activity, was not necessary for bipolar bud-site selection (Figure S2). Therefore, we concluded that the EKC/KEOPS complex is involved in bipolar bud-site selection with a signaling pathway different from the Sch9p kinase.

EKC/KEOPS complex is involved in the regulation of Bud9p localization

We showed that *BUD9* deletion in the *bud32Δ*, *cgi121Δ*, and *gon7Δ* mutants suppressed random budding and increased budding at the distal pole. In concordance with these results,

Table 3 Localization patterns of GFP-Bud9p

	Unbudded cells			Budded cells				
	Proximal	Both poles	No signal	Proximal	Bud neck	Proximal/neck	No signal	Others
BY4743	12	5	83	10	7	9	71	3
bud32Δ	3	0	97	<1	3	<1	96	0
cgi121Δ	2	0	98	2	0	3	95	0
gon7Δ	1	0	99	3	1	4	92	0

Each value indicates the percentage of total cells.

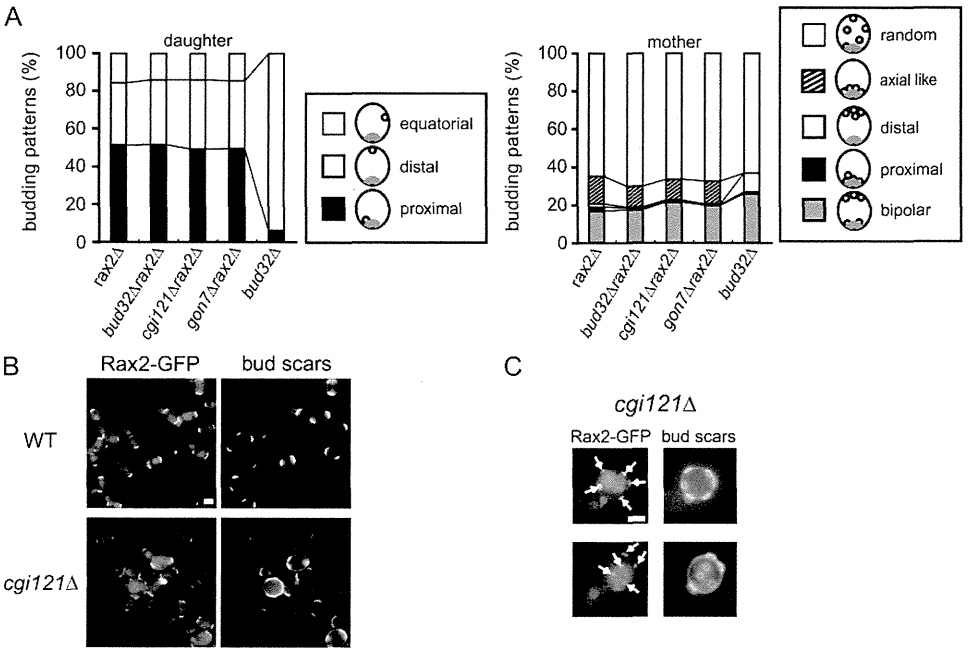

Figure 4 Genetic interaction between *RAX2* and *EKC/KEOPS* genes. (A) Budding pattern of cells with deletion of *RAX2* in the *bud32Δ*, *cgi121Δ*, and *gon7Δ* mutant backgrounds. Strains used were the diploid wild type (BY4743), *rax2Δ* (CCY044), *bud32Δrax2Δ* (CCY046), *cgi121Δrax2Δ* (CCY048), *gon7Δrax2Δ* (CCY051), and *bud32Δ* (CCY003). Budding positions are classified as in the budding pattern of diploid cells in Figure 1A. At least 150 cells were scored for each bud scar pattern from both daughter and mother cells (the percentages are indicated). In daughter cells, the solid, open, and dotted boxes indicate cells with buds at only the proximal pole, at only the distal pole, and at a random site, respectively. In mother cells, the shaded, solid, open, slashed, and dotted boxes indicate cells with buds at two poles, only the proximal pole, only the distal pole, axial-like and at random sites, respectively. (B) Diploid wild type (CCY034) and *cgi121Δ* (CCY038) expressing Rax2p-GFP from their own promoter at their chromosomal locus were grown overnight to log phase in YPD liquid medium, stained with calcofluor white, and then suspended in water for observation. Rax2p-GFP and bud scars were observed with a fluorescence microscope with GFP and UV filter sets, respectively. Bar, 5 μm. (C) Bud scars at the equatorial position of random budding sites were also marked by Rax2p-GFP. The arrows indicate Rax2p-GFP localization at random positions. Bar, 5 μm.

Bud9p localization was affected by deletion of *BUD32*, *CGI121*, and *GON7* (Figure 3D and Table 3). The deletion of *BUD8* did not suppress random budding of *bud32Δ*, *cgi121Δ*, and *gon7Δ* mutants although proximal budding increased in the double mutants in place of the distal budding observed in the single mutants (Figure 2B). The proximal budding in the mutants might be due to the accidental localization of Bud9p at the proximal pole because Bud9p is expressed in a normal amount in these cells (Figure 3E).

Our data suggest that mislocalization of Bud9p by loss of the EKC/KEOPS components caused random budding. Proper localization of Bud9p is also dependent on the timing of *BUD9* expression that was observed in the G1 phase (Schenkman *et al.* 2002). A possibility exists that the EKC/KEOPS complex might be related to the timing of *BUD9* expression because the complex controls transcription of several genes (Kisseleva-Romanova *et al.* 2006). In a promoter swapping assay, GFP-Bud9p expression from the *BUD8* or *CLB2* promoter specifically at the G2/M phase failed to rescue unipolar proximal budding in a *bud9Δ-1* mutant, indicating inefficient delivery or poor stability of Bud9p, or both (Schenkman *et al.* 2002). Furthermore,

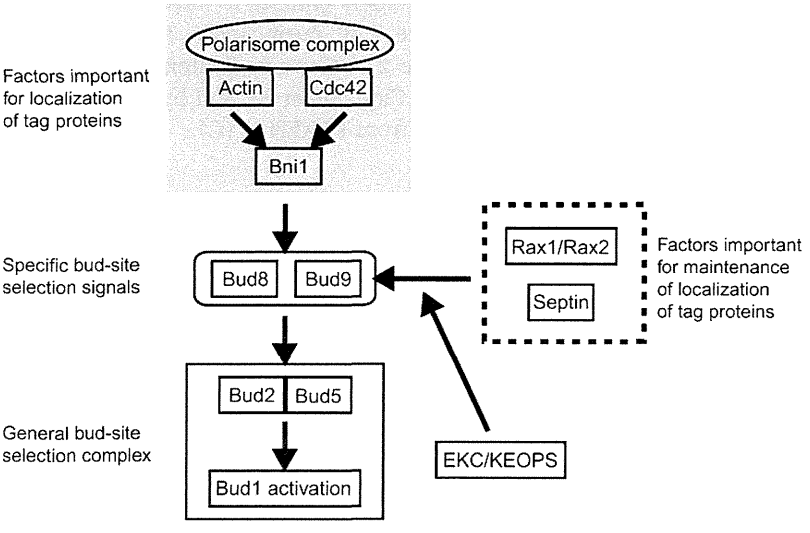

Figure 5 Regulation of the localization of the bipolar markers Bud8p and Bud9p by the EKC/KEOPS complex and Rax1p/Rax2p. The schematic illustration is based on figure 3 in Casamayor and Snyder (2002). For details, see the Discussion.

virtually no random budding was seen in these cases. Localization of GFP-Bud9p in *bud32*Δ, *cgi121*Δ, and *gon7*Δ mutants was observed in a dot-like structure at cell periphery, as shown in Figure 3D. We confirmed that the stability and expression level of Bud9p were the same as that of the wild type (Figure 3E). GFP-Bud9p from the *BUD8* promoter in the *bud9*Δ*-1* mutant appeared to localize in internal vesicles, and the mutant showed mainly unipolar distal budding (Schenkman *et al.* 2002). If the time lag for *BUD9* expression occurs in the *bud32*Δ, *cgi121*Δ, and *gon7*Δ, it should largely be unipolar distal budding not random budding. Therefore, we conclude that random budding in the mutants is caused by mislocalization at the cell periphery after delivery of Bud9p to the plasma membrane, but not through a time lag in *BUD9* expression. Support for this conclusion was also provided by our observation that GFP-Bud8p localization patterns in the mutant deleted of each EKC/KEOPS component were similar to those of the wild type because the delivery of both Bud8p and Bud9p to the presumptive bud site is dependent on actin (Schenkman *et al.* 2002).

The deletion of *RAX2* in diploid cells induced random budding and axial-like budding, although ~20% of cells showed a bipolar budding pattern. Axial budding was suppressed in diploid cells, as Axl1p, on which axial budding is dependent, is transcriptionally repressed in diploid cells (Fujita *et al.* 1994). However, the allele mutant of both *BUD8* and *BUD9* uses axial budding cues (Zahner *et al.* 1996). Several components of the axial budding system, such as Axl2p and Bud3p, are also expressed in diploid cells. Indeed, *BUD3* deletion in the *bud8*Δ*bud9*Δ double mutant essentially induces a random budding pattern (Harkins *et al.* 2001). Axial budding cues can be recognized with less efficiency in diploid cells when both bipolar markers are impaired. However, we never observed an axial-like budding pattern in the deletion mutant of EKC/KEOPS components (Figure 1 and Figure 2). This indicates that the axial budding system is essentially inactive in these cells although a very small part of the bud at the proximal pole might use such a cue.

We observed that deletion of *RAX2* in *bud32*Δ, *cgi121*Δ, and *gon7*Δ mutants changed the phenotype to one identical with *rax2*Δ (Figure 4A). In concordance with this observation, Rax2p distribution did not differ between the wild type and *bud32*Δ, *cgi121*Δ, or *gon7*Δ (Figure 4, B and C, and Figure S3). We also confirmed that regulation of Bud9p localization by the EKC/KEOPS complex is independent of septin by observing the localization of Cdc11p-GFP, one of the septin subunits, in the deletion mutant of the EKC/KEOPS component (Figure S4). These results suggest that the EKC/KEOPS complex acts to regulate Bud9p localization as a downstream factor of Rax2p and septin.

Regulation of bipolar bud-site selection by the EKC/KEOPS complex

We concluded that the EKC/KEOPS complex in diploid cells acts as a Rax2p downstream factor and that the complex maintains bipolar budding through regulation of Bud9p localization (Figure 5). The localization of the cortical markers Bud8p and Bud9p is regulated by several proteins as shown in Figure 5. The EKC/KEOPS complex is the factor regulating the localization of only Bud9p, downstream of Rax2p and septins. Recent reports suggest that the complex functions in telomere maintenance, transcriptional regulation, and t^6A modification (Downey *et al.* 2006; Kisseleva-Romanova *et al.* 2006; Daugeron *et al.* 2011; Srinivasan *et al.* 2011), although direct target of the complex is still elusive. The complex localized mainly to the nucleus, and the minor portion of the EKC/KEOPS complex localized to cytosol (Y. Kato, H. Kawsaki, and H. Hirano, unpublished data), whereas Bud9p localized to the cell surface. Although the complex in the cytosol might be directly linked to Bud9p, we could not observe a physical interaction between these proteins. These results suggest that the regulation of Bud9p localization by the complex may not occur at the cell surface and that the localization of Bud9p might be regulated by factor(s) under the transcriptional control by the EKC/KEOPS complex. Further experiments, such as suppressor screening that can rescue Bud9p localization in the deletion mutants of each EKC/KEOPS component, might be able to identify the factors that are important for establishing and maintaining spatial cues in cells.

Our results suggest that the correct localization of Bud9p is essential for bipolar budding. Although many of the genes that specifically caused random budding when deleted are associated with the localization of Bud8p, so far no genes have been reported that specifically regulate only Bud9p, except for the septins (Ni and Snyder 2001; Schenkman *et al.* 2002). Our findings revealed that the EKC/KEOPS complex is specifically involved in the regulation of Bud9p localization. Further analysis of this regulation system will be an important step toward understanding asymmetric development from spatial cues in diploid cells.

Acknowledgments

We thank Nobuyuki Endo (Keyence Corporation) for technical advice on the BIOREVO BZ-9000 fluorescence microscope. We are also extremely grateful to Katsuaki Asano for his assistance with the TAP purification. This work was partly supported by the 21st Century Centers-of-Excellence Program at Yokohama City University and by Grants-in-Aid for Scientific Research from KAKENHI (C).

Literature Cited

Ausubel, F. M., R. Brent, R. E. Kingston, D. D. Moore, J. G. Seidman, *et al.*, eds. 1995 *Current Protocols in Molecular Biology.* John Wiley & Sons, New York.

Bedinger, P. A., K. J. Hardeman, and C. A. Loukides, 1994 Travelling in style: the cell biology of pollen. Trends Cell Biol. 4: 132–138.

Casamayor, A., and M. Snyder, 2002 Bud-site selection and cell polarity in budding yeast. Curr. Opin. Microbiol. 5: 179–186.

Chant, J., and J. R. Pringle, 1995 Patterns of bud-site selection in the yeast *Saccharomyces cerevisiae*. J. Cell Biol. 129: 751–765.

Chant, J., M. Mischke, E. Mitchell, I. Herskowitz, and J. R. Pringle, 1995 Role of Bud3p in producing the axial budding pattern of yeast. J. Cell Biol. 129: 767–778.

Chen, T., T. Hiroko, A. Chaudhuri, F. Inose, M. Lord, *et al.*, 2000 Multigenerational cortical inheritance of the Rax2 protein in orienting polarity and division in yeast. Science 290: 1975–1978.

Christianson, T. W., R. S. Sikorski, M. Dante, J. H. Shero, and P. Hieter, 1992 Multifunctional yeast high-copy-number shuttle vectors. Gene 110: 119–122.

Daugeron, M. C., T. L. Lenstra, M. Frizzarin, B. EL Yacoubi, X. Liu, *et al.*, 2011 Gcn4 misregulation reveals a direct role for the evolutionary conserved EKC/KEOPS in the t6A modification of tRNAs. Nucleic Acids Res. (in press).

Downey, M., R. Houlsworth, L. Maringele, A. Rollie, M. Brehme, *et al.*, 2006 A genome-wide screen identifies the evolutionarily conserved KEOPS complex as a telomere regulator. Cell 124: 1155–1168.

Drubin, D. G., and W. J. Nelson, 1996 Origins of cell polarity. Cell 84: 335–344.

Freifelder, D., 1960 Bud position in *Saccharomyces cerevisiae*. J. Bacteriol. 80: 567–568.

Fujita, A., C. Oka, Y. Arikawa, T. Katagai, A. Tonouchi, *et al.*, 1994 A yeast gene necessary for bud-site selection encodes a protein similar to insulin-degrading enzymes. Nature 372: 567–570.

Gietz, D., A. St. Jean, R. A. Woods, and R. H. Schiestl, 1992 Improved method for high efficiency transformation of intact yeast cells. Nucleic Acids Res. 20: 1425.

Halme, A., M. Michelitch, E. L. Mitchell, and J. Chant, 1996 Bud10p directs axial cell polarization in budding yeast and resembles a transmembrane receptor. Curr. Biol. 6: 570–579.

Harkins, H. A., N. Page, L. R. Schenkman, C. De Virgilio, S. Shaw, *et al.*, 2001 Bud8p and Bud9p, proteins that may mark the sites for bipolar budding in yeast. Mol. Biol. Cell 12: 2497–2518.

Hirano, H., 1989 Microsequence analysis of winged bean seed proteins electroblotted from two-dimensional gel. J. Protein Chem. 8: 115–130.

Hyman, A. A., and J. G. White, 1987 Determination of cell division axes in the early embryogenesis of *Caenorhabditis elegans*. J. Cell Biol. 105: 2123–2135.

Kang, P. J., A. Sanson, B. Lee, and H. O. Park, 2001 A GDP/GTP exchange factor involved in linking a spatial landmark to cell polarity. Science 292: 1376–1378.

Kang, P. J., E. Angerman, K. Nakashima, J. R. Pringle, and H. O. Park, 2004 Interactions among Rax1p, Rax2p, Bud8p, and Bud9p in marking cortical sites for bipolar bud-site selection in yeast. Mol. Biol. Cell 15: 5145–5157.

Kato, Y., N. Arakawa, Y. Masuishi, H. Kawasaki, and H. Hirano, 2009 Mutagenesis of longer inserts by the ligation of two PCR fragments amplified with a mutation primer. J. Biosci. Bioeng. 107: 95–97.

Kawasaki, H., A. Okayama, Y. Iwafune, S. Yahagi, N. Arakawa, *et al.*, 2008 Multiplex detection and identification of proteins on a PVDF membrane blocked with a synthetic polymer-based reagent. Electrophoresis 29: 4377–4380.

Kisseleva-Romanova, E., R. Lopreiato, A. Baudin-Baillieu, J. C. Rousselle, L. Ilan, *et al.*, 2006 Yeast homolog of a cancer-testis antigen defines a new transcription complex. EMBO J. 25: 3576–3585.

Krappmann, A. B., N. Taheri, M. Heinrich, and H. U. Mosch, 2007 Distinct domains of yeast cortical tag proteins Bud8p and Bud9p confer polar localization and functionality. Mol. Biol. Cell 18: 3323–3339.

Kraut, R., W. Chia, L. Y. Jan, Y. N. Jan, and J. A. Knoblich, 1996 Role of inscuteable in orienting asymmetric cell divisions in Drosophila. Nature 383: 50–55.

Kruger, N. J., 1994 The Bradford method for protein quantitation. Methods Mol. Biol. 32: 9–15.

Longtine, M. S., and A. McKenzie III, D. J. Demarini, N. G. Shah, A. Wach, *et al.*, 1998 Additional modules for versatile and economical PCR-based gene deletion and modification in *Saccharomyces cerevisiae*. Yeast 14: 953–961.

Mao, D. Y., D. Neculai, M. Downey, S. Orlicky, Y. Z. Haffani, *et al.*, 2008 Atomic structure of the KEOPS complex: an ancient protein kinase-containing molecular machine. Mol. Cell 32: 259–275.

Mooseker, M. S., 1985 Organization, chemistry, and assembly of the cytoskeletal apparatus of the intestinal brush border. Annu. Rev. Cell Biol. 1: 209–241.

Ni, L., and M. Snyder, 2001 A genomic study of the bipolar bud site selection pattern in *Saccharomyces cerevisiae*. Mol. Biol. Cell 12: 2147–2170.

Park, H. O., and E. Bi, 2007 Central roles of small GTPases in the development of cell polarity in yeast and beyond. Microbiol. Mol. Biol. Rev. 71: 48–96.

Peggion, C., R. Lopreiato, E. Casanova, M. Ruzzene, S. Facchin, *et al.*, 2008 Phosphorylation of the *Saccharomyces cerevisiae* Grx4p glutaredoxin by the Bud32p kinase unveils a novel signaling pathway involving Sch9p, a yeast member of the Akt/PKB subfamily. FEBS J. 275: 5919–5933.

Roosen, J., K. Engelen, K. Marchal, J. Mathys, G. Griffioen, *et al.*, 2005 PKA and Sch9 control a molecular switch important for the proper adaptation to nutrient availability. Mol. Microbiol. 55: 862–880.

Sanders, S. L., and I. Herskowitz, 1996 The BUD4 protein of yeast, required for axial budding, is localized to the mother/BUD neck in a cell cycle-dependent manner. J. Cell Biol. 134: 413–427.

Schenkman, L. R., C. Caruso, N. Page, and J. R. Pringle, 2002 The role of cell cycle-regulated expression in the localization of spatial landmark proteins in yeast. J. Cell Biol. 156: 829–841.

Srinivasan, M., P. Mehta, Y. Yu, E. Prugar, E. V. Koonin, *et al.*, 2011 The highly conserved KEOPS/EKC complex is essential for a universal tRNA modification, t6A. EMBO J. 30: 873–881.

Stocchetto, S., O. Marin, G. Carignani, and L. A. Pinna, 1997 Biochemical evidence that *Saccharomyces cerevisiae* YGR262c gene, required for normal growth, encodes a novel Ser/Thr-specific protein kinase. FEBS Lett. 414: 171–175.

Taheri, N., T. Kohler, G. H. Braus, and H. U. Mosch, 2000 Asymmetrically localized Bud8p and Bud9p proteins control yeast cell polarity and development. EMBO J. 19: 6686–6696.

Zahner, J. E., H. A. Harkins, and J. R. Pringle, 1996 Genetic analysis of the bipolar pattern of bud site selection in the yeast *Saccharomyces cerevisiae*. Mol. Cell. Biol. 16: 1857–1870.

Communicating editor: M. D. Rose